An Examination of the Nature and Dynamics of Seismogenesis in South California, USA, based on Non-Extensive Statistical Physics

Angeliki Efstathiou and Andreas Tzanis

Section of Geophysics, Department of Geology and Geoenvironment,
National and Kapodistrian University of Athens;
aefstathiou@geol.uoa.gr; atzanis@geol.uoa.gr

Reference: Efstathiou, A. and Tzanis, A., 2018. An examination of the nature and dynamics of seismogenesis in South California, USA, based on Non-Extensive Statistical Physics, *Physics of the Earth and Planetary Interiors*, 284**,** 51–71; doi: 10.1016/j.pepi.2018.08.013

August 2018

Abstract

We examine the nature of the seismogenetic system in South California, USA, by searching for evidence of complexity and non-extensivity in the earthquake record. We attempt to determine whether earthquakes are generated by a self-excited Poisson process, in which case they are independent, or by a Critical process, in which long-range interactions in non-equilibrium states are expected (correlation). Emphasis is given to background seismicity, i.e. to the rudimentary expression of the seismogenetic system. We use the complete and homogeneous earthquake catalogue published by the South California Earthquake Data Centre, in which aftershocks are either included, or have been removed by a stochastic declustering procedure. We examine *multivariate* cumulative frequency distributions of earthquake magnitudes, interevent time and interevent distance in the context of Non-Extensive Statistical Physics, which generalizes the additive Boltzmann-Gibbs thermodynamics to non-additive (non-extensive) dynamic systems. Our results indicate that the seismogenetic systems of South California are generally sub-extensive complex and certainly non-Poissonian. Background seismicity exhibits long-range interaction as evidenced by the overall increase of correlation observed by declustering the earthquake catalogues, as well as by the high correlation observed for earthquakes separated by long interevent distances. The results compare very well with those obtained in previous work for the seismogenetic systems of North California. Specifically, the Walker Lane – Eastern California Shear Zone on one hand, and the San Andreas Fault system – south California Continental Borderland region on the other, appear to comprise fault networks with different dynamics and expression. The former exhibits persistent, very high correlation and has attributes of (stationary) Self-Organized Criticality (SOC). The latter exhibits high correlation mainly at long ranges and has attributes of evolutionary of (Self-Organized) Criticality. All in all, our results are compatible with simulations of small-world fault networks in which free boundary conditions at the surface allow for self-organization and criticality to develop.

1. INTRODUCTION

Seismicity generally comprises processes that generate a mixture of earthquake populations: the *background* that expresses the continuum of regional tectonic deformation and the *foreground* that expresses the prolific local short-term activity associated with aftershocks and aftershock sequences. These have traditionally been described with the statistics-based models of statistical seismology. Over the past two decades, however, physically-based statistical modelling of seismicity has attracted growing attention. This approach uses statistical physics in order to bridge the gap between physics-based models of individual events (without statistics), and statistics-based models of event populations (without physics); it endeavours to generate the statistical models from first principles, respecting the laws of thermodynamics and taking into account physical laws such as those of friction, rupture etc. In other words, it uses physics to support stochastic models, a quality often missing from traditional statistical seismology. The development of theoretical and experimental methods and techniques that combine the physics and statistics of seismogenesis has led to two general conceptual frameworks.

The first postulates that the expression of the seismogenetic background process is Poissonian in time and in space and obeys Boltzmann-Gibbs thermodynamics; it is expressed by a series of well-known models suggesting that background earthquakes are statistically independent and although it is possible for one event to trigger another, this occurs in an unstructured random way and does not contribute to the long-term evolution of seismicity. The most influential of these models, which is based on the self-excited conditional Poisson process, is ETAS (Episodic Type Aftershock Sequence, e.g. Ogata, 1998, 1988; Zhuang et al, 2002; Helmstetter and Sornette, 2003; Touati et al, 2009; Segou et al, 2013; many others). ETAS posits that randomly occurring earthquakes trigger aftershocks and aftershocks trigger their own aftershocks, thus spawning a short-term proliferation of clustered events (aftershock sequences) whose number decays according to the Omori-Utsu power-law (e.g. Utsu et al., 1995). Point process models to address the problem of intermediate to long-term clustering have also been developed, such as the PPE (Proximity to Past Earthquakes; Marzocchi and Lombardi, 2008), the EEPAS (Each Earthquake is a Precursor According to Scale; Rhoades, 2007), as well as their variants and derivatives.

Poissonian models are mainly concerned with the statistics of time and distance between events. The size (magnitude) distribution of earthquakes still obeys the Gutenberg and Richter (1944) frequency–magnitude (F-M) law which, however, is a power-law that *cannot* be derived from the Boltzmann-Gibbs formalism. Likewise, the Omori-Utsu formula is a Zipf-Mandelbrot power-law and inconsistent with the Boltzmann-Gibbs formalism. The reliance of Poissonian seismicity models on irrefutable but evidently non-Poissonian empirical laws is an apparent contradiction with no theoretical resolution; it shows that they effectively are *ad hoc* constructs attempting to reconcile the (inherited) Poissonian

worldview of statistical seismology with the non-Poissonian dynamics of fault formation and aftershock clustering.

The second framework comprises different classes of models proposing that seismicity expresses a complex, non-equilibrating fractal fault network (system). One well-known such class of models proposes that seismicity continuously evolves toward a stationary critical state with no characteristic spatiotemporal scale, in which instabilities –namely earthquakes– develop spontaneously and have a chance of cascading into large (global scale) events. This is the concept of Self Organized Criticality (SOC, e.g. Bak and Tang, 1989; Sornette and Sornette, 1989; Olami et al., 1992; Sornette and Sammis, 1995; Rundle et al., 2000; Bak et al, 2002; Bakar and Tirnakli, 2009; etc.). The allure of SOC is that it is self-consistent and also predicts several observed properties of earthquake occurrence: the Gutenberg-Richter law and the Omori-Utsu law emerge *naturally* during the evolution of simulated fault networks. A variant of SOC is Self-*Organizing* Criticality, which leads to Critical Point behaviour at the end of an earthquake cycle (e.g. Sornette and Sammis, 1995; Rundle et al., 2000; Sammis and Sornette, 2001; many others). This has been influential in the late 1990's and early 2000's but is no longer pursued as its predictions could not be statistically verified. In the context of Criticality, the dependence between successive earthquakes (faults) is known as *correlation*, involves long-range interaction and endows the seismogenetic system with memory that should be manifested with power-law statistical distributions of energy release, temporal dynamics and spatial dependence. A few authors investigated models with alternative complexity mechanisms that do not involve criticality yet maintain the fault system in a state of non-equilibrium, a list of which can be found in Sornette (2004) and Sornette and Werner (2009). Notable among these is the Coherent Noise Model (Newman, 1996), shown by Celikoglu et al., (2010) to generate power-law behaviour in the time dependence of successive events, but has a rather weak point in that it does not include some geometric configuration of "faults".

Both Poissonian and Complex/Critical viewpoints agree that the foreground process comprises a set of dependent events, although the former assign only local significance to this dependence, while the latter consider them to be integral part of the regional process. Their fundamental difference lies in their understanding of the background process: the former assumes that it generates statistically independent earthquake populations (no correlation, no memory, exponential distributions of temporal and spatial dynamic parameters), while the latter requires short and long-range interactions that generate statistically dependent populations (correlation, power-law distributions). It therefore stands to reason that if it were possible to identify and eliminate the foreground, one would be able to explore the nature and dynamics of the background provided that one would implement effective measures of correlation and analyse them on the basis of a *natural* self-consistent general theoretical framework and not with model-based or ad hoc conceptual constructs.

In what can be thought of as "prequels" to the present work, Tzanis et al., (2013, 2018) and Efstathiou et al., (2015, 2016, 2017) addressed the question of the statistical nature of seismicity by using the theoretical context of Non Extensive Statistical Physics to analyse empirical multivariate distributions (joint probabilities) of earthquake frequency as a function of magnitude and time/distance between successive events (measures of correlation); the distributions were constructed on the basis of complete and homogeneous earthquakes catalogues in which aftershocks were either present (full catalogues), or had been removed with the stochastic declustering method of Zhuang et al., (2002). That work included concise analyses of seismicity along the boundary of the North American and Pacific plates in California (transformational) and Alaska (transformational and convergent), as well as thorough analyses of seismicity in North California and along the San Andreas Fault (Efstathiou et al., 2015; 2017). Herein we expand that work by conducting a thorough analysis of South Californian seismicity based on the same concepts and techniques. For the sake of brevity, the reader will be referred to Efstathiou et al., (2017), and Tzanis et al., (2018) whenever the need for details may arise. However, in order to preserve the autonomous character, completeness and comprehensibility of the present work, we succinctly provide all of the necessary information, including basic theoretical concepts, the fundamentals of the analytical techniques and brief explanations/justification of basic choices and assumptions.

2. NON-EXTENSIVE APPROACH TO EARTHQUAKE STATISTICS

2.1 Multivariate (joint) probability distributions

A definite indicator of interaction between faults is the lapse between consecutive earthquakes above a magnitude threshold and over a given area: this is referred to as *interevent time, waiting time, calm time*, *recurrence time* etc. Understanding the statistics of earthquake frequency vs. interevent time (F-T) is essential for understanding the dynamics of the fault network. Empirical F-T distributions generally exhibit power-law characteristics with fat tails. For this reason, in the context of classical statistical seismology, they have been analysed with tailed standard statistical models reducible to power laws in some way or another, as for instance are the gamma and Weibull distributions (e.g. Bak et al., 2002; Davidsen and Goltz, 2004; Corral, 2004; Martinez et al, 2005; Talbi and Yamazaki, 2010). Some researchers working from a statistical physics perspective, proposed ad hoc mechanisms for the generation of power laws by a combination of correlated aftershock and uncorrelated background processes (e.g. Saichev and Sornette, 2013; Touati et al, 2009; Hainzl et al, 2006). Nevertheless, Molchan (2005) has shown that for a stationary point process, if there is a universal distribution of interevent times, then it must be exponential! A second measure of fault interaction is the *hypocentral distance* between consecutive earthquakes above a magnitude threshold and over a given area (*interevent distance*). The statistics of the frequency vs. interevent distance (F-D) should be

related to the *range of interaction* and is not fully understood, as it has been studied very few researchers (e.g. Eneva and Pavlis, 1991; Abe and Suzuki, 2003; Batak and Kantz, 2014; Shoenball et al., 2015). Finally, a third criterion of correlation (albeit seldom acknowledged as one), is the *b* value of the Gutenberg–Richter law which expresses the scaling of the size-space of active faults over a given area (fault hierarchy) and conveys information about their spatial distribution and the homogeneity of the domain they occupy. The F-M distribution is *static* and does not say much about the dynamics of the fault network, or about correlations in the energy released by successive earthquakes. Nevertheless, it is an undisputable standard against which to compare physical and statistical descriptions of the scaling of earthquake sizes: as such it will be used herein.

As in our previous work, (Efstathiou et al., 2017; Tzanis et al., 2018; etc.), the earthquake occurrence model is based on the bivariate joint Frequency – Magnitude – Interevent Time (F-M-T) distribution that expresses the joint probability of observing an earthquake above of given magnitude and interevent time within a given range of interevent distances. In order to construct a bivariate F-M-T distribution, a cut-off magnitude M_{th} is set and a bivariate frequency table (histogram) representing the *incremental* F-M-T earthquake count (frequency) is first compiled. The empirical *cumulative* frequency is then obtained by backward bivariate summation according to the scheme $N_{m\tau} = \sum_{j=D_T}^{\tau} \sum_{i=D_M}^{m} \left\{ H_{ij} \Leftrightarrow H_{ij} \neq 0 \right\}$, $\tau = 1,\ldots D_T$, $m = 1,\ldots D_M$, where H is the incremental frequency, D_M is the dimension of H along the magnitude axis and D_T is the dimension of H along the Δt axis. It is worth noting that the cumulative F-M-T distribution is formed by stacking *only* the populated (non-zero) bins of the incremental distribution; the necessity of this constraint is thoroughly explained in Efstathiou et al., (2017) and Tzanis et al., (2018). An example of such a construct is shown in Fig. 1a and in logarithmic frequency scale (solid circles). The data has been extracted from the *full* catalogue of the South California Earthquake Data Center for the period 1980-2015 and for $M_{th} \geq 3.75$ (see Section 3.2 for details).

As a general rule, F-M-T distributions comprise well-defined and structured surfaces, with their end-member at [$M \geq M_{th}$, Δt=0] comprising the one-dimensional Gutenberg–Richter law and the opposite end member at [M_{th}=0, Δt] comprising the one-dimensional Frequency – Interevent Time (F-T) function. The cumulative frequency (earthquake count) can be written thus: $N(\{M \geq M_{th}, \Delta t : M \geq M_{th}\})$. It follows that, the empirical probability $P(>\{M \geq M_{th}, \Delta t : M \geq M_{th}\})$ is simply

$$\frac{N(>\{M \geq M_{th}, \Delta t : M \geq M_{th}\})}{N(M_{th}, 0)}, \quad N(M = M_{th}, 0) = \left\| N \right\|_{\infty}. \qquad (1)$$

Complexity and self-organization are associated with long-range interactions and long-term memory; these attributes are referred to as *correlation*. Conversely, Poissonian processes are local and memory-less, i.e. uncorrelated. The study of F-M-T distributions will provide information with respect to the size distribution and memory of the seismogenetic system for the range over which the distribution is

constructed. In order to study the dependence of correlation on different ranges, we use the *interevent distance*, i.e. the hypocentral distance between consecutive earthquakes, as a spatial filter by which to separate and study the temporal correlation of proximal and distal earthquakes: the premise is that if distal earthquakes are correlated in time, then they have to be correlated in space by long-distance interaction and vice versa. In consequence, we also analyse F-M-T distributions based on data subsets grouped by interevent distance according to the rule

$$C \supset \{C_D: M > M_{th} \wedge \Delta d_L \leq \Delta d \leq \Delta d_U\}, \quad (2a)$$

where C is the catalogue, C_D is the subset catalogue, Δd is the interevent distance and Δd_L, Δd_U are the upper and lower group limits. This, is equivalent to constructing and modelling the *conditional* bivariate cumulative distribution

$$P(> \{M \geq M_{th}, \Delta t : [M \geq M_{th} \wedge \Delta d_L \leq \Delta d \leq \Delta d_U]\}) \quad (2b)$$

as a proxy of the *trivariate* F-M-T-D distribution.

2.2 NESP formulation of F-M-T joint distributions

Non-Extensive Statistical Physics (NESP) is a fundamental theoretical framework developed to account for non-additive (non-equilibrating) systems in which the total (systemic) entropy does not equal to the sum of the entropies of their components. NESP has been introduced by Constantino Tsallis (Tsallis, 1988, 2001; 2009; Tsallis and Tirnakli, 2010) as a generalization of the Boltzmann-Gibbs thermodynamics. In statistical mechanics, an N-component dynamic system may have $W=N!/\Pi_i N_i!$ microscopic states, where i ranges over all possible conditions (states). In classical statistical mechanics, the entropy of that system S is related to the totality of these microscopic states by the Gibbs formula $S=-k\sum_i p_i \ln(p_i)$, where k is the Boltzmann constant and p_i is the probability of each microstate. If the components of the system are all statistically independent (non-interacting), the entropy of the system factorises into the product of N identical terms, one for each component; this is the Boltzmann entropy $S_B=-Nk\sum_i p_i \ln(p_i)$. It is easy to see that one basic property of the Boltzmann-Gibbs entropy is *additivity* (*extensivity*): the entropy of the system equals the sum of the entropy of its components. Recently, it has been recognized that a very broad spectrum of non-equilibrating natural and physical systems does not conform to this requirement. Such *non-additive* systems, commonly referred to as *non-extensive*[1] after Tsallis (1988), include *statistically dependent* (interacting) components that bestow memory and can no longer be described with Boltzmann-Gibbs (BG) statistical physics.

In NESP terms, the non-equilibrium states of some dynamic parameter x can be described by the Tsallis (1988) entropic functional:

[1] The term "extensive" (full/ complete according to Merriam-Webster's definition), was used by Tsallis (1988) to designate systems that are equilibrating, as opposed to those that are not (incomplete, i.e. non-extensive). The terms "additive" and "non-additive" are probably more appropriate but we shall henceforth use Tsallis's terminology for consistency with international literature.

$$S_q = k\frac{1}{q-1}\left[1-\int_W p^q(x)dx\right], \quad (3)$$

where $p^q(x)dx$ is the probability of finding its value in $[x, x+dx]$ so that $\int_W p^q(x)dx = 1$, k is the Boltzmann constant and q is the *entropic index*. For q=1, Eq. 3 reduces to the well-known Boltzmann–Gibbs functional $S_{BG} = -k\int_W p(x)\ln\left(p(x)\right)dx$. The Tsallis entropy is concave and fulfils the *H*-theorem but is not additive when $q \neq 1$; for a mixture of two statistically independent systems *A* and *B*, it satisfies $S_q(A, B) = S_q(A) + S_q(B) + (1-q)\, S_q(A)\, S_q(B)$. This property is known as *pseudo-additivity* and is further distinguished into *super-additivity* (*super-extensivity*) if $q<1$, *additivity* when $q=1$ and *sub-additivity* (*sub-extensivity*) if $q>1$. Accordingly, the entropic index is a measure of *non-extensivity*.

By maximizing S_q, it can be shown that when $q>0$ and $x \in [0, \infty)$, the *cumulative* probability function (CDF) of x is the *q-exponential distribution* (Tsallis, 1988, 2009; Abe and Suzuki, 2005)

$$P(>x) = \exp_q\left(-\frac{x}{x_0}\right) = \left[1-(1-q)\left(\frac{x}{x_0}\right)\right]^{\frac{1}{1-q}} \quad (4)$$

where x_0 is a characteristic value (*q- relaxation* value) of x and

$$\exp_q(x) = \begin{cases} (1+(1-q)x)^{\frac{1}{1-q}} & 1+(1-q)x > 0 \\ 0 & 1+(1-q)x \le 0 \end{cases},$$

is the *q-exponential* function, such that for q=1, $\exp_q(x) = e^x$. As apparent in Eq. 4, for sub-extensive systems with $q>1$, $P(>x)$ is a power-law with tail. For extensive (random) systems with q=1, $P(>x)$ is an exponential distribution. Finally, for super-extensive systems with $0<q<1$, $P(>x)$ is a power-law with a cut-off so that $P(>x)=0$ whenever the argument becomes negative; such systems are characterized by bounded correlation radii.

NESP has already been applied to the statistical description of seismicity with noteworthy results; for thorough reviews see Efstathiou et al., (2017) or Tzanis et al., (2018). Interevent times are real and positive and it is straightforward to see that the CDF expressed by Eq. 4 is the only NESP formulation applicable to the analysis of F-T distributions. The case of the F-M distribution is more complicated in that it has to be derived from Eq. 3 in a manner relating the energy stored in faults with the (scaled) measure of the energy released by earthquakes, i.e. the magnitude. This was pioneered by Sotolongo-Costa and Posadas (2004) and refined by Silva et al., (2006) and Telesca (2011, 2012); it is a first principles approach based on NSEP-compatible "fragment-asperity models" that consider the interaction of asperities and the fragments filling space between them, (which is supposed to modulate earthquake triggering). Such models differ in their assumption of how the energy stored in the asperities and fragments scales with their characteristic linear dimension. We assert that the F-M distribution model proposed by Telesca (2011, 2012), which assumes that the energy scales with the area of the fragments and asperities ($E \propto r^2$) so that $M \propto \frac{2}{3}\log(E)$, is consistent with the empirical

laws of energy–moment and moment–magnitude scaling and is also compatible with the well-studied rate-and-state friction laws of rock failure. Accordingly, the F-M distribution used herein is

$$P(>M)=\frac{N(>M)}{N_0}=\left(1-\frac{1-q_M}{2-q_M}\cdot\frac{10^{2M}}{\alpha^{2/3}}\right)^{\left(\frac{2-q_M}{1-q_M}\right)}, \qquad (5)$$

with the constant α expressing the proportionality between the released energy E and the fragment size r and q_M is the *magnitude entropic index*.

The distributions of magnitude M and interevent time Δt are generated by independent processes so that the joint probability $P(M \cup \Delta t)$ can factorize into the probabilities of M and Δt:

$$P(M \cup \Delta t) = P(M)\, P(\Delta t). \qquad (6)$$

On combining equations (1), (4), (5) and (6), removing the normalization and taking the logarithm one obtains

$$\log N\left(>\{M \geq M,\ \Delta t : M \geq M\}\right) =$$
$$= \log(N_{M=0}) \quad + \quad \left(\frac{2-q_M}{1-q_M}\right)\cdot\log\left(1-\frac{1-q_M}{2-q_M}\cdot\frac{10^M}{\alpha^{2/3}}\right) \quad + \quad \frac{1}{1-q_T}\log\left(1-\Delta t_0^{-1}(1-q_T)\Delta t\right) \qquad (7)$$

where q_M, q_T are entropic indices for the magnitude and interevent times respectively and Δt_0, is the *q-relaxation time*, analogous to the relaxation time often encountered in the analysis of physical systems. Eq. 7 is a generalized (bivariate) Gutenberg – Richter law in which

$$b_q = \frac{(2-q_M)}{(q_M-1)} \qquad (8)$$

is the NESP *generalization* of the b value and comprises the general model to be implemented herein.

The parameters of Eq. 7 can be approximated with non-linear least-squares. Because they are all positive and the entropic indices are bounded, we have chosen to implement the *trust-region reflective* algorithm (e.g. Moré and Sorensen, 1983; Steihaug, 1983), together with *least absolute residual* (LAR) minimization so as to suppress possible outliers. An example is shown in Fig. 1a. The quality of the approximation (continuous surface) is excellent with a correlation coefficient R^2 ≈0.99. The magnitude entropic index q_M = 1.52±0.002 so that b_q≈0.94, which compares well to the b values computed with conventional one-dimensional techniques for the same data set (see Fig. 3). The temporal entropic index q_T is approximately 1.44 ±0.018 and indicates significant sub-extensivity. Fig. 1b presents a succinct statistical appraisal of the result, performed by fitting a normal location-scale distribution (dashed line) and a Student-t location-scale distribution (solid line) to the cumulative probability of the sorted residuals (r). Approximately 93.3% of the residual population, for which -0.23 ≤ r ≤ 0.16, is normally distributed. The tails forming at r< -0.23 and r >0.16 are fairly well fitted with the t-location-scale distribution; they comprise only 6.7% of the population and represent statistically expected outliers which have been effectively suppressed by the LAR procedure.

3. EARTHQUAKE DATA

3.1 Source areas

The present study focuses on the seismicity of southern California, USA. The study area will henceforth be referred to as the South California Seismic Region or SCSR. The northern boundary of the SCSR is the WNW-ESE oriented Santa Ynez and Garlock Fault zones; it begins at the western terminus of the Santa Ynez Fault Zone – Pacific Section which is a virtual extension of the Garlock fault (34.5°N, -120.5°E); then it runs south of Tejon Pass and parallel to the Garlock Fault up to approximately (35.5°W, -116.3°E) the past its eastern terminus (Mojave Desert). The boundary then turns to the south and runs eastward of the South Bristol Mts. Fault (34.6°N, -115.6°E), to approximately (32.0°N, -114.5°E) in the Gran Desierto de Altar (Sonora, Mexico), north of the head of the Gulf of California; it continues westwards to approx. (32°N, -117°E), which is south of Tijuana, Mexico, and then to (32°N, -119°E) off the west coast of Mexico. Finally, it turns north and runs parallel to the coastline and west of the San Clemente and Santa Cruz Islands up to 34.5°N.

The SCSR is characterized by several major faults and numerous branches that create a complex landscape of seismic activity. Different earthquake source areas are included in the analysis, as illustrated in the composite seismicity map of Fig. 2 and elaborated below:

a) The southern part of the East California Shear Zone (ECSZ) extends south of the Garlock Fault and runs across the Mojave Desert, terminating upon the San Andreas Fault system between Salton Lake and the San Bernardino Mts. It is a zone of strike-slip faults that accommodates approximately 25% of the total motion between the North American and Pacific plates (Dixon et al., 2000; Miller et al., 2001) and has generated some of the largest earthquakes of South California, such as the 1992 Landers earthquake (M_w=7.3) and the 1999 Hector Mine earthquake (M_w=7.1). The eastern expanse of the ECSZ is delimited by the diffuse extensional deformation of the Basin and Range province. Although the origin of the ECSZ is still open to debate, it has been suggested that it was formed by northward propagation of the plate boundary in the Gulf of California due to the northward motion of the Baja California microplate (Faulds et al., 2005a,b; Harry, 2005; McCrory et al., 2009). According to Plattner et al., (2009, 2010) and Li and Liu (2006), the geometrical complexity of the San Andreas fault system, along with the accommodation of shear strain from the interaction of the Baja microplate and North American plate, is a key component of this zone's formation.

b) The Inner Continental Borderland region (ICB) contains several faults and extends offshore and to the west of the southern California mainland, from Point Conception to the Vizcaíno Peninsula in Baja California. The area comprises a complex tectonic system in which seismicity appears to be more diffuse than in the mainland even for events associated with main-shock sequences, although this may be an artefact of lopsided network geometry and structural heterogeneity (Astiz and

Shearer, 2000; references therein). The area can be divided into four major sub-parallel groups of dextral faults which, from east to west are: i) the Newport–Inglewood (NIF) and Rose Canyon (RCF) faults that make landfall at San Diego and perhaps connect with the Vallecitos and San Miguel faults in Baja California; ii) the Palos Verdes (PVF) – Coronado Bank (CBF) fault that makes landfall near Ensenada, Mexico; iii) the Santa Cruz – Santa Catalina – San Diego Trough – Bahia Soledad (SDTF) fault that makes landfall south of Punta, Mexico; iv) the Santa Cruz – San Clemente – San Isidro fault zone (SCF). During the past 50 years, several moderate (M_L 5 to 6) earthquakes have occurred in the region, consistent with the right-lateral deformation of the local Pacific–North American plate boundary and the regional tectonics of the San Andreas Fault system (e.g., Weldon and Humphreys 1986). Some of those, however, had significant dip-slip components including the largest recorded offshore event, the 1951 San Clemente Island earthquake (M_L=5.9).

c) Sandwiched between the ECSZ and the ICB is the San Andreas Fault system (sSAF). This is a trilateral system of large sub-parallel faults comprising the southern segment of the San Andreas Fault in the east and its sibling San Jacinto fault (SJF) in the centre and the Elsinore fault (EF) in the west. San Jacinto fault is considered to be one of the most active in South California as it accounts for 75% of the slip rate between the Pacific and North American plates and has generated moderate to large earthquakes in the past. The Elsinore fault runs parallel to San Jacinto and has been considerably less active in historic times. To the north, the sSAF system terminates against the left-lateral Garlock fault, a major tectonic boundary believed to have developed in order to accommodate the strain differential between the almost W-E extension of the Great Basin eastwards of the ECSZ (e.g. Wernicke et al., 1988), and the NW-SE right lateral transformation of the ECSZ and SAF. Thus, the right-lateral motion on the SAF and ECSZ locks up in the area of the Garlock, where local variations in the mode of deformation and earthquake focal mechanisms are observed (e.g. Jones, 1988; Hardebeck and Hauksson, 2001; Fialko, 2006; Becker et al, 2005). Between 37.7°N and 35.1°N, the left-lateral motion of the Galrlock fault generates a restraining bend and a broad S-shaped westward displacement of the SAF, known as the "Big Bend". The southern boundary of the sSAF, if any, is not clearly defined. The eponymous fault terminates at the southeast corner of the Salton Sea but is thought to connect with the Imperial Fault though the extensional Brawley Seismic Zone (BSZ). The San Jacinto and Elsinore faults are also thought to extend to the SE, with San Jacinto also terminating against the Imperial Fault and Eslinore continuing into Mexico as the Laguna Salada Fault (LSF), in which the M7.2 Baja California of 2010 has occurred. It is interesting to observe that there is a zone of aligned earthquake activity that appears to commence at the terminus of sSAF at Salton Sea, run in an average N220° direction along the south coast of Salton Sea, pass along a N40° zone of short fault strands associated with the San Jacinto–Superstition Hills segment (active in historic times), then between

the N220° left-lateral Yuha Wells fault (active in the Late Quaternary) and the N220° "unnamed faults north of Coyote Wash" of unspecified kinematics but active in the last 15ka (e.g. Jennings, 1994), and continue south-westward crossing the coastline just north of Ensenada, Mexico. This "*Unspecified Seismic Zone*" discontinues seismic activity between the Elsinore and Laguna Salada faults and is better observed with the 2016 upgrade of the relocated catalogue of Hauksson et al., (2012); because any horizontal motion there can only be left-lateral, one is tempted to *ponder* whether it is a fault zone that serves as a barrier against the Laguna Salada and Imperial faults and thus delimiting the southward extent of the SCSR (a southern "lesser Garlock" so to speak).

3.2 Earthquake catalogues

The earthquake data was extracted from the regional earthquake of the South California Earthquake Data Centre (SCEDC @ http://www.data.scec.org) for the area 36ºN to 32ºN and -122ºE to -114ºE, and the period 1968 to 2017. As reported in Hutton et al., (2010), as of the early 1930's and up to the early 1970's the SCSN network was sparse and consisted of about 49 stations. As a result, the epicentral distribution maps compiled for the broader area of South California projected an image of somewhat diffuse seismicity. During the 1980's and early 1990's the network improved qualitatively and quantitatively: more than 100 additional stations were installed, while past events were relocated and magnitudes re-determined. With denser network and modern data processing, it became clear that earthquakes activity was mainly clustered along and around the large active faults of the Late Quaternary (Fig. 2). As can be seen in Fig. 3a, the sustainable magnitude of completeness (M_c) was approximately 3.0 during the early to mid-1970s and decreased after 1975 so as to attain a sustainable level of approximately 2.5 as of the early 1980's. The spiky fluctuations observed in Fig. 3a correspond to time-local instabilities caused by major aftershock sequences and should not be viewed as temporary changes in the detection threshold.

In the SCSN catalogue most earthquakes are reported in the M_L and M_w magnitude scales while there is a considerable number of events reported in the duration (M_d) and amplitude (M_x) scales. Eaton (1992) has calibrated M_d and M_x against the M_L scale and has shown that they are within 5% of the M_L scale for magnitudes in the range 0.5 to 5.5, as well as virtually independent of the distance from the epicentre to at least 800 km. In consequence, M_d and M_x are practically equivalent to M_L. For the purpose of the present analysis M_w magnitudes were converted to M_L using the empirical formula of Uhrhammer et al., (1996): $M_w = M_L \times (0.997 \pm 0.020) - (0.050 \pm 0.131)$. Given these adjustments, for the period 1968-2017 the catalogue is complete for magnitudes $M_L \geq 3$ and comprises 10793 events (Fig. 3b) while for the period 1980-2017 it is complete for $M_L \geq 2.5$ and comprises 30117 events (Fig. 3c).

The question of whether the background seismogenetic process is inherently random or correlated may be answered by analysing reduced versions of the earthquake catalogue, in which aftershock

sequences are eliminated in an optimal as possible way. The process of reducing an earthquake catalogue by separating background and foreground events is referred to as *declustering*. We have chosen to implement the declustering method of Zhuang et al. (2002) because it has significant for our objectives advantages (for details see Efstathiou et al., 2017): i) it optimizes the temporal and spatial window in which to search for aftershocks by fitting an ETAS model to the earthquake data; ii) it assigns each earthquake in the catalogue with a probability that it is an aftershock of its predecessor so that all earthquakes may be possible main shocks to their short-term aftereffects, and, iii) it is a *paradigmatic* realization of the self-excited Poisson process. Thus, if the background seismicity obeys Boltzmann-Gibbs statistics, this method should be able to extract a nearly random background process against which to test the alternative hypotheses. If it is does not, the argument in favour of non-Poissonian background would be stronger. The algorithm assigns a probability ϕ_j for the j^{th} event in the catalogue to belong to the background or foreground processes and thus separates the catalogue into a series of sub-processes whose initiating events comprise the background. As a rule of thumb, an event with $\phi_j \leq 50\%$ is taken to be foreground while an event with $\phi_j > 50\%$ is likely to belong to the background.

The results of the declustering exercise are summarized in Table 1 and an example of the resulting cumulative earthquake counts for the period 1968-2017 ($M_c \geq 3$) is given in Fig. 4. It is apparent that at the $\phi \geq 70\%$ probability level the catalogue is *almost* free of the time-local rate jumps that indicate the presence of aftershock sequences, therefore it is fairly representative of the background process. It is natural to expect that at this probability level a small portion of events will be residuals of the foreground process which, however, are progressively eliminated at higher probability levels. Fig. 5 illustrates the epicentral distributions of the full and declustered catalogues used herein. Thus, Fig. 5a shows the epicentres of the full catalogue for the period 1968-2017 and $M_c \geq 3.0$ and Fig. 5b, 5c and 5d its declustered realizations at probability levels $\phi \geq 70\%$, $\phi \geq 80\%$ and $\phi \geq 90\%$ respectively. Likewise, Fig. 5e shows the full catalogue for the period 1980-2017 and $M_c \geq 2.5$ and Fig. 5f, 5g and 5h its declustered realizations at probability levels $\phi \geq 70\%$, $\phi \geq 80\%$ and $\phi \geq 90\%$ respectively. The full and declustered catalogues for the period 1980-2017 contain more events than the corresponding catalogues of the period 1968-2017 due to the lower magnitude of completeness. It is also clear that background earthquake activity is compactly distributed along the major faults of the ICB, sSAF and ECSZ source areas, a point that will be of importance in explaining the results of the analysis presented in Section 4. It is equally clear that the declustering procedure has classified *all* major earthquakes to the foreground, as can be easily ascertained by observing, say Fig. 5a/5b and Fig. 5e/5f.

4. RESULTS

The analysis and appraisal of our results will be based on the fact that NESP predicts *correlation* (dependence) between earthquakes, which involves long-range interaction, endows the seismogenetic system with memory and generates power-law statistical distributions of its dynamic parameters. The degree of correlation is measured by the entropic indices so that if $q \neq 1$, the system is non-extensive, whereas if $q \to 1$ the system is Poissonian (uncorrelated and memoryless). Because the appraisal of low-valued experimental realizations of q can be ambiguous for obvious reasons, we also require a measure (threshold) on the basis of which to confidently infer whether a seismogenetic system is non-extensive or Poissonian.

The answer to the above question lies in the determination of randomness thresholds, i.e. the value above which it is safe to accept that the temporal entropic index q_T indicates non-extensive seismogenetic processes. This exercise has been undertaken by Efstathiou et al. (2015; 2017) for the South and North Californian seismicities respectively; it is repeated herein for the sake of completeness and robustness. Accordingly, we apply Eq. 7 to the analysis of several background catalogues generated on the basis of the ETAS model, using the stochastic aftershock simulator program "AFTsimulator" by Felzer (2007): each of these should yield temporal entropic indices with an expectation value of unity. The program uses the Gutenberg-Richter and Omori-Utsu laws to simulate the statistical behaviour of background and foreground seismicity, and Monte Carlo methods to simulate background earthquakes as well as multiple generations of aftershocks. This leads to the generation of realistic synthetic background catalogues, consistent with the known long-term seismotectonic characteristics of a given area (for details see Felzer et al., 2002 and Felzer and Brodsky, 2006). The implementation was based on the ETAS parameterization obtained (fitted) by declustering the SCSN *and* NCSN catalogues; it also assumed uniform background seismicity rates such that b=1, and a maximum expected magnitude of M_L=7.3, the same as the maximum observed in California over the 49-year period 1968-2017 (the Landers earthquake of 1982).

Fig. 6 illustrates the analysis of 40 synthetic background catalogues: 20 for the entire SCSR source area and, for the sake of comparison, 20 for the entire seismic region of North California. Fig. 6a shows the variation of the mean values $\langle q_M \rangle$ and $\langle q_T \rangle$ computed from the analysis of all synthetic catalogues and their associated 3σ error margins, as a function of the threshold (or cut-off) magnitude M_{th}. It is apparent that all $\langle q_T(M_{th}) \rangle$ are consistently lower than 1.1, indicating very low correlation – effectively randomness – without exception. Likewise, all $\langle q_M(M_{th}) \rangle$ exhibit an almost imperceptible variation around 1.5, so that $b_q \approx 1$, consistently with the assumptions on which the synthetic ETAS catalogues were constructed. It is also apparent that the populations $\{q_T(M_{th})\}$ and $\{q_M(M_{th})\}$ from which $\langle q_T(M_{th}) \rangle$ and $\langle q_M(M_{th}) \rangle$ have been derived are remarkably consistent: the 3σ error level is

generally very small and in most cases smaller in size than the symbols representing the expectation values! Fig. 6b illustrates the variation of entropic indices computed by grouping the earthquakes of the synthetic catalogues according to interevent distance (Eq. 2). The results have been derived by considering all earthquakes above a magnitude threshold M_{th} =3.0 and as above, the panel illustrates mean values $\langle q_M(\Delta d)\rangle$, $\langle q_T(\Delta d)\rangle$ and 3σ error margins. Again as above, all $\langle q_T(\Delta d)\rangle$ are consistently low for all interevent distance groups, so that $\max[\langle q_T(\Delta d)\rangle + 3\sigma] \leq 1.2$, while $\langle q_M(\Delta d)\rangle$ are also very stable and exhibit small fluctuations around 1.5, so that $b_q \rightarrow 1$ as expected. In consequence of this analysis, as well as those of Efstathiou et al. (2015, 2017), it can safely be concluded that the estimation procedure yields stable magnitude entropic indices, absolutely consistent with the assumptions on which the synthetic ETAS catalogues were constructed, and that experimental values $q_T(M_{th}) \geq 1.15$ and $q_T(\Delta d)\rangle > 1.2$ would be compelling evidence of non-extensive seismogenetic dynamics.

Last but not least, we should mention why the temporal entropic indices obtained from the synthetic ETAS catalogues deviate from unity, although by very little (after all, Efstathiou et al., 2017 demonstrated that $q \approx 1$ in the case of truly Gaussian univariate sequences). The answer is that the AFTsimulator draws random numbers from a *uniform* distribution. On the other hand, experimental realizations of q_T computed on the basis of Eq. 7 can be arbitrarily close to unity *only* for truly random interevent time data. When uniformly distributed data is used, and given the local nature of least-squares solvers, the minima of the parameter space are expected to move away from unity by small, albeit not always insignificant distances, thus generating the variability observed in Fig. 6. Conversely, the distribution of magnitudes in the synthetic catalogues is made to follow the Gutenberg-Richter law; as a result, q_M does not exhibit variability. Although we have identified this issue early on, we chose not to adjust the original AFTsimulator code even if this meant that we had to "sacrifice" perfectly legitimate low-valued temporal entropic indices. We made this decision because we felt that we had to establish a very rigorous criterion, which would ensure that whatever inference we made would be trustworthy and hard to contend.

As already discussed in Section 3.2, the SCSN catalogue has improved significantly in response to improvements in the detection threshold of the seismological network and in analytical procedures, with particular reference to the period after 1980. Accordingly, in order to be as thorough as possible and ensure the significance of our results, we conducted comparative analyses of full earthquake catalogues for the entire SCSR and individual source areas defined in Section 3.1, for two overlapping periods: 1968-2017 with a threshold magnitude $M_{th} \geq 3$, and 1980-2017 with a threshold magnitude $M_{th} \geq 2.5$. The analysis focused on the variation of the entropic indices with respect to threshold magnitude (M_{th}) and interevent distance (Δd). The results are summarized in Table 2 and illustrated in Figures 7 to 13. In order to maintain experimental rigour, estimation of the entropic indices is *not* performed for catalogue subsets containing *less than* 500 events and results are *not* considered and

displayed *unless* associated with a goodness of fit (R^2) *better* than 0.97.

4.1 Full catalogue analysis

As can be seen in Fig. 7, the magnitude entropic indices are consistently determined and that the experimental $q_M(M_{th})$ functions computed for each of the source areas are remarkably comparable for both periods and all threshold magnitudes. For the SCSR and sSAF catalogues, $q_M(M_{th})$ varies from 1.5 at M_{th}=2.5 (b_q=1) to 1.49 (b_q=1.04) at M_{th}=3.0, steadily increasing thereafter to 1.59 at M_{th}=4.3 (b_q=0.7). The entropic index q_M, like the *b*-value to which it is related, represents the scaling of the size distribution of earthquakes. Here it indicates a *sub-extensive* scale-free process associated with gradual changes in the size distribution of small-intermediate magnitude events that appear to become progressively more clustered. For the ECSZ area, $q_M(M_{th})$ is stably determined around a mean value of 1.5 ($1.49< q_M(M_{th}) <1.53$), so that and $b_q(M_{th}) \in (0.88, 1.04)$. For ICB and $M_{th}>3.0$, $q_M(M_{th})$ is slightly higher for the period 1968-2017 ($1.51<q_M(M_{th})<1.54$) than for 1980-2017 when in varies between 1.48 and 1.49; given that the ICB is mainly offshore, this may be an effect of the post-1975 improvement of the SCSN network.

The variation of q_M with interevent distance Δd is shown in Fig. 8. It is again apparent that $q_M(\Delta d)$ remains stable over all interevent distances and is very consistent for all periods and source areas, generally varying between 1.47 and 1.56 so that $b_q(\Delta d)$ would vary between 1.12 and 0.78. Small differences of the order of 0.01–0.03 can be observed only at short interevent distances (Δd <100 km) in the results of the SCSR and sSAF catalogues, in which $q_M(\Delta d)$ is slightly higher for the period 1968-2017 (M_{th}=3.0) than for 1980-2017 (M_{th}=2.5). We consider these very small to be of physical consequence; they may likely be an effect of the post-1975 improvements in the detecting network. Changes in scaling analogous to those observed in Fig. 7 are not evident because the threshold magnitudes used in these calculations are considerably lower than the magnitude threshold of the changes.

The variation of the temporal entropic index with threshold magnitude is shown in Fig. 9. Beginning with the SCSR full catalogues, it is apparent that for both periods $q_T(M_{th})$ is lower than 1.2 at small magnitude scales, but for $M_{th} \geq 3.6$ steadily increases to values above 1.5 at magnitudes $M_{th} \geq 4$ (strong sub-extensivity). If taken over the *entire* SCSR area, small earthquakes appear to be uncorrelated, possibly because very small events are *locally* and prolifically spawned by different parental earthquakes at distal locations; these have no causal relationship and when mixed and chronologically ordered in a catalogue, they may randomize the statistics of interevent times. It is thus interesting to point out the increase of correlation with magnitude, which we interpret as an effect of the increasing interaction (correlation) radii associated with increasingly larger events. Similar results are obtained from the sSAF full catalogues, although here the increase of $q_T(M_{th})$ begins at M_{th}=3.6 and is much

steeper; this may indicate strong fault-fault interactions within the sSAF system, which commence at some critical(?) interaction radius and escalate rapidly. The ICB source area exhibits analogous behaviour with the difference that the increase in correlation commences as early as M_{th} =2.9, where $q_T \approx 1.22$, and appears to rise smoothly to approximately 1.5 at M_{th}=3.3; beyond this point earthquake numbers drop to levels that do not guarantee statistical rigour. The ECSZ full catalogues yield rather different results: $q_T(M_{th})$ is rather stably determined around a mean value of 1.8±0.03 for $M_{th} \leq 3.0$, and jumps to 1.95±0.03 for $M_{th} \geq 3.1$. The ECSZ fault system appears to be pervasively and intensely correlated and to be persistently sub-extensive; these properties render it different from the sSAF and ICB systems, as will further be discussed below.

The variation of the temporal entropic index with *interevent distance* (Δd) is shown in Fig. 10. When the analysis is carried out in this mode, it is expected that $q_T(\Delta d)$ will exhibit high values at interevent distances shorter than 100km due to the dominant effect of near field interaction, with particular reference to aftershock sequences. This is generally observed for all $q_T(\Delta d \leq 100\text{km})$ so that $1.6 < q_T \leq 1.95$. For Δd >150km the results of the SCSR catalogues indicate very low correlation (q_T <1.2) except at the longest interevent distances (Δd>300km). The longitudinal and latitudinal linear dimensions of the SCSR are comparable and of the order of 450km. Given the considerably smaller longitudinal dimensions of the ECSZ, sSAF and ICB, as well as the results of Fig. 10b-d, the increase in the value of q_T observed for Δd>300km may indicate interaction *across* the three source areas (let alone that such interevent distances have usually nothing to do with aftershock sequences). For the sSAF catalogues, $q_T(\Delta d)$ is consistently lower than 1.15 for all Δd >100km. However, given that $M_{th} \leq 3$, it is straightforward to see that the results are dominated by the overwhelming majority of uncorrelated small magnitude events, consistently with the analysis presented in Fig. 9. If the threshold magnitude is increased, then the correlation increases over all interevent distances, also in consistency with the analysis of Fig. 9. As can be seen in Fig. 10a, the analysis of the SCSR 1980-2017 full catalogue with M_{th} = 3.8, shows that $q_T(\Delta d$=50km) increases from 1.59 to 1.81 and $q_T(\Delta d$=100km) from 1.12 to 1.7; likewise, for Δd >100km q_T varies from 1.26 at Δd=200km to 1.16 at Δd>300km, albeit with a persistent tendency to decrease. Thus, the SCSR system can be shown to exhibit long range correlation. Unfortunately, these results cannot be repeated for higher threshold magnitudes, or for the sSAF source area, due to diminishing numbers of earthquakes per Δd group (and corresponding reduction in statistical significance). In the ICB source area correlation appears to increase to moderate levels (1.2 – 1.3) at long interevent distances (Δd>150km). Finally in the ECSZ, the correlation is persistently strong ($1.54 < q_T \leq 1.73$) over all Δd >50km; given that the longest linear dimension of the ECSZ is of the order of 200km, the results indicate that correlation is uniformly strong over all ranges.

Based on the analysis of both $q_T(M_{th})$ and $q_T(\Delta d)$, it is quite apparent that the ICB and sSAF fault networks, which effectively comprise sub-parallel segments and branches of the Pacific – North American transformational plate boundary, exhibit analogous statistical behaviour and dynamics. The ECSZ system is different: it appears to exist in a state of extremely high correlation over all interevent distances (long range correlation), a feature that can hardly be understood in terms other than Self-Organized Criticality. Notably, a rather similar result has been obtained by Efstathiou et al., (2017) for the source area of Walker Lane – Sierra Nevada Range of North California. It stands to reason that being a southward continuation of the Walker Lane, the ECSZ should exhibit analogous seismogenetic dynamics the origin of which, as well as the origin of the differences between ECSZ and the rest of SCSR, is open to debate. In a final comment, we note that the results obtained for the periods 1968-2017 and 1980-2017 are absolutely compatible. Accordingly, the analysis of declustered catalogues shall be based on the catalogue of the latter (1980-2017) period only, which may span a shorter interval (36.5 years instead of 48.9), but is complete for magnitudes lower than the former (1968-2017).

4.2 Declustered catalogue analysis

A primary objective of our study is to investigate whether background seismicity is generated by non-Poissonian dynamic processes. Accordingly, we proceed to examine declustered versions of the SCSR, sSAF, ICB and ECSZ catalogues, in which aftershock sequences have been identified and removed by the stochastic declustering method of Zhuang et al (2002) at probability levels $\phi \geq 0.7$ and $\phi \geq 0.8$ for an event to belong to the background. It must be noted that the analysis of entropic indices with respect to interevent distance will be limited to SCSR and sSAF, because in the other catalogues the small populations of events left at interevent distances longer than 50km do not guarantee the statistical significance of the $q_M(\Delta d)$ and $q_T(\Delta d)$.

Fig. 11 illustrates the results obtained from the SCSR catalogue. As can be seen in Fig. 11a, q_M does not fluctuate with M_{th} and is very consistently determined around 1.5 ±0.0095 and 1.51 ±0.006 for probabilities ≥0.7 and ≥0.8 respectively, so that $b_q \approx 1$. Likewise, $q_M(\Delta d)$ is practically featureless and stable around 1.5±0.015 and 1.51±0.0075 for probabilities ≥0.7 and ≥0.8 respectively (Fig. 11c), so that b_q is again approximately equal to unity. Interesting observations can be made only in regard to the temporal entropic index. In Fig. 11b, it is apparent that for probabilities $\phi \geq 0.7$, q_T is *consistently* greater than 1.4 for $2.5 < M_{th} < 3.6$, which represents a very significant increase in comparison to the correlation observed at the same magnitude range of the full catalogue (Fig. 9a). As per Fig. 9a, increase of q_T with magnitude is also observed, only that here it commences as early as M_{th}=2.8 where q_T=1.44 and culminates at M_{th}=3.5 where $q_T \approx 1.8$. By raising the probability level to $\phi \geq 0.8$, $q_T(M_{th})$ increases and fluctuates between 1.6 and 1.7 so as to average at 1.66±0.035. It is significant to note that the increase of q_T with magnitude disappears. Given that aftershocks have practically been

eliminated at this probability level, the result can be taken to indicate a seismogenetic background that is very strongly correlated at all magnitude scales. Analogous observations can be made on $q_T(\Delta d)$. For $\phi \geq 0.7$, q_T cannot be determined at the required level of rigour when Δd <100km (Fig. 11d). However, it clearly increases from 1.64 at Δd=100km to 1.77 at Δd=250km and averages to 1.70±0.064, which represents an increase of 0.57 in comparison to the corresponding results of the full SCSR catalogue (Fig. 10a). For $\phi \geq 0.8$ and Δd<100km, q_T is 1.59±0.02, approximately the same with the corresponding determination of the full SCSR catalogue. It is therefore conceivable that strong short-range correlation (near field interaction) persists in the background. For $\phi \geq 0.8$ and $\Delta d \geq$100km, q_T rises to above 1.7, having an average value of 1.76± 0.04 (Fig. 11d). As a general conclusion, the results of both probability levels indicate sub-extensivity and very strong long range correlation in the seismogenetic background of the *entire* SCSR area.

Let us, now, examine the declustered sSAF catalogue, for which results are shown in Fig. 12. It is apparent that the variation of the entropic indices with magnitude and interevent distance is very similar to that of the declustered SCSR area. Again, q_M does *not* fluctuate with M_{th} and averages to 1.52±0.009 for $\phi \geq 0.7$ and 1.51±0.004 for $\phi \geq 0.8$ (Table 2 and Fig. 12a). Perfectly analogous results are obtained for the variation of q_M with interevent distance (Table 2 and Fig. 12c). As with SCSR, interesting observations can be made only in regard to the temporal entropic index. Thus, for $\phi \geq 0.7$ q_T is generally greater than 1.5 when 2.5< M_{th} <3.3 (Fig. 12b), which constitutes a *very* significant increase in comparison to the correlation observed in the same magnitude range of the full catalogue (Fig. 9a). Increase of q_T with magnitude is again observed commencing at M_{th}=2.7 and culminating at M_{th}=3.3 ($q_T \approx 1.75$). For $\phi \geq 0.8$, $q_T(M_{th})$ varies between 1.62 and 1.73 with an average of 1.68 ±0.048; as with SCSR (Fig. 11b), this indicates a background with the same high level of correlation at all magnitude scales. Turning now to Fig. 12d, it is apparent that q_T exhibits an upward trend with increasing interevent distance. For $\phi \geq 0.7$ it steadily increases from 1.5 at Δd=50km to 1.75 at Δd=225km and averages to 1.63±0.096; this represents an increase of 0.52 in comparison to the corresponding results of the full catalogue (Fig. 10b). For $\phi \geq 0.8$, q_T rises from 1.62 at Δd = 50km to above 1.79 at $\Delta d \geq$175km, attaining an average value of 1.77±0.1. Once again, one may assert that the results of both probability levels indicate sub-extensivity and very strong long-range correlation in the sSAF background which, given its relatively narrow longitudinal dimension (~100km), should mainly be attributed to processes taking place lengthwise of the main seismogenetic faults.

The variation of the entropic indices with magnitude for the declustered ECSZ and ICB catalogues is shown in Fig. 13. As evident in Fig. 13a and 13c, the magnitude entropic indices are featureless and practically identical, averaging to 1.51±0.01 in both cases. For $\phi \geq 0.7$ the temporal entropic index of ECSZ exhibits clear increase, beginning with 1.63 at M_{th}=2.5 and ending with 1.78 for M_{th}=3 (Fig. 13b); for $\phi \geq 0.8$ q_T is seen to fluctuate between 1.8 and 1.9 without exhibiting some trend (Fig. 13b).

Such q_T values are very similar to those obtained from the full ECSZ catalogue at the same magnitude scales and confirm that background seismogenesis is thoroughly and strongly correlated. The temporal entropic index of the ICB source area can be determined only for magnitude thresholds between 2.5 and 2.7, and only at the $\phi \geq 0.7$ probability level. Nonetheless, it can be observed to fluctuate between 1.6 and 1.8, averaging at 1.74 (Fig. 13d); when compared to the average obtained for the full ICB catalogue at the same magnitude scales, q_T has increased by an astounding 0.62. Once again, this is compelling evidence that background seismogenesis in ICB is throughout sub-extensive and strongly correlated.

The analysis of catalogues declustered at the $\phi \geq 0.9$ probability level is summarized in Table 2. Results are shown only for SCSR and sSAF, as the declustered ECSZ and ICB catalogues respectively contain 441 and 290 events and cannot be reliably evaluated. $q_M(M_{th})$ and $q_M(\Delta d)$ have values very similar to those obtained at the 80% probability level (see above) and as well, exhibit very little variation. Likewise, $q_T(M_{th})$ for SCSR and sSAF, as well as of $q_T(\Delta d)$ for sSAF, persist at the same high levels, and appear to exhibit the same type of variation as in the case of the $\phi \geq 0.8$ probability level.

In concluding this Section, our analysis has shown that on removing aftershock sequences, the seismogenetic systems of South California exhibit very high levels of correlation (long-term memory and long-range interaction). On the basis of this evidence it is possible to infer that they are inherently non-Poissonian, as will further be discussed below (Section 5).

5. DISCUSSION AND CONCLUSIONS

The present study is part of a continued attempt to examine the statistical nature and dynamics of seismogenesis by using Non-Extensive Statistical Physics (NESP) to search for evidence of complexity and correlation (fault-fault interaction) in bivariate cumulative distributions of earthquake magnitudes and interevent times. Herein, we study the seismogenetic system(s) of South California, USA, by examining the entire South California Seismic Region, as well fault sub-networks identified according to their geotectonic setting (see Section 3.1): the Eastern California Shear Zone (ECSZ), the southern segment of the San Andreas fault system (sSAF) and the Inner Continental Borderland area (ICB). In all cases aftershocks sequences are either included (full catalogues), or eliminated (declustered catalogues) using the stochastic declustering method of Zhuang et al. (2002). As discussed in Section 2, and more thoroughly in previous work (Efstathiou et al., 2017; Tzanis et al., 2018), NESP is an appropriate tool by which to determine whether seismogenesis comprises a self-excited conditional Poisson process, or a Complex process that continuously develops into a critical state. The distinguishing factor is *correlation*. Whereas the former concept posits that earthquake occurrence comprises fundamentally independent (uncorrelated) events that do not influence the

evolution of the fault network over large scales and long ranges, the latter posits that earthquakes are statistically dependent (correlated) over long spatiotemporal distances due to unavoidable long range fault-fault interactions. NESP predicts that the existence of correlation may be assessed by the *magnitude* (q_M) and *temporal* (q_T) entropic indices that indicate the extent of fault-fault interaction (see Section 2.2). More precisely, q_T indicates the extent to which earthquakes may stimulate the occurrence of their successor events, i.e. the internal dynamics of the fault network. The threshold above which it is safe to assume non-Poisson statistical physics was determined in Section 3.2, where it was found that $q_T \geq 1.15$ would generally comprise incontestable evidence for the existence of correlation.

Turning to the discussion of our results we note that in full and declustered catalogues the magnitude entropic index q_M is generally stable between 1.48 ($b_q \approx 1.1$) and 1.54 ($b_q \approx 0.85$), with the exception of the full sSAF catalogue where it exhibits a systematic upward trend from approximately 1.52 ($b_q=0.96$) at $M_{th}=3.1$ to 1.59 at $M_{th}=4.2$ ($b_q \approx 0.7$); the average q_M is 1.52 ± 0.027 ($b_q=0.92$). These results are consistent with the Gutenberg-Richter law given that b_q is congruent with the b value and that $b_q=1$ when $q_M=1$. Moreover, as amply demonstrated by Efstathiou et al., (2015, 2017), b_q values determined with the procedure described in Section 2.2 are consistent with b values computed with conventional methods. This is important because the G-R law *cannot* be derived in the context of point (Poisson) processes, but *can* be derived from *first principles* in the generalized context of NESP (Section 2.2). Accordingly, in terms of the size distribution and scaling, the South Californian fault networks can be classified as *sub-extensive complex* with a high degree of self-organization. An interesting observation is of the systematic increase of q_M in sSAF (and possibly ICB) for $M_{th} \geq 3.1$. This would imply that the clustering of earthquake foci increases with magnitude so that the fault network becomes progressively more compact and the crust more homogeneous. We are inclined to attribute this effect to natural and not technical causes (e.g. better localizability of larger magnitude events), because it does not appear in the ECSZ. We consider more likely that in the related sSAF/ICB source areas, larger earthquakes are located closer to the principal faults on which the bulk of slip (deformation) is concentrated.

Let us, now, focus on the dynamics of South Californian seismicity as indicated by the temporal entropic index q_T computed for the period 1980-2017, beginning with the results of the full catalogues. A first observation is that if only small magnitude thresholds are considered, sSAF and ICB would appear to be almost Poissonian for $M_{th} \leq 2.9$ (Fig. 9b, 9c) and $\Delta d \geq 100$km (Fig.10b, 10c). However, for $M_{th}>3.5$ in sSAF and $M_{th}>2.7$ in ICB, correlation increases at the rather similar rates of 0.62 and 0.55 per magnitude unit respectively. Moreover, for $M_{th}>4$ correlation becomes very strong in sSAF (q_T >1.6, Fig. 9b) and although it is not possible to determine what happens in ICB, it is likely that it becomes at least as strong. In addition, at interevent distances transcending the linear dimensions of individual source areas, the fault networks of SCSR appear to be at least weakly correlated (Fig. 10a).

As first discussed in Section 4.1, we suggest that small earthquakes, whose numbers overwhelm the catalogues, may be uncorrelated because they have very short interaction radii and their majority is spawned by different parental earthquakes at distal locations of the seismogenetic area. Accordingly, distal small earthquakes belonging to filial generations of localized activity have no causal relationship and when mixed and chronologically ordered in a catalogue, randomize the statistics of interevent times. In this view, the increase of correlation with magnitude can be interpreted as an effect of progressive increase of interaction radii associated with of progressively larger events, as well as of the nature of the fault network (see below). This interpretation is corroborated by the observation that when the threshold is increased, correlation becomes significant at interevent distances greater than, or equal to 100km (Fig. 10a). ECSZ appears to be profoundly different in that very intense correlation is observed at all magnitude scales and interevent distances of ECSZ (average $q_T(M_{th})$ = 1.92 ±0.07). This suggests that the profound differences between ECSZ and ICB/sSAF may also have to do with the nature, dynamic state and even the size of the fault network, as will be further elaborated below.

On removing the aftershock sequences *increased* correlation is observed in SCSR, sSAF ICB, both with respect to threshold magnitude as with respect to interevent distance; the increase is *very* significant –more than 0.5 – and affects all magnitude scales and interevent distances; the level of correlation appears to increase with the the probability of events to belong to the background (Fig. 11 and 12). At probability levels ≥80% $q_T(M_{th})$ stabilizes at levels between 1.6 and 1.8. The effect is reverse in the ECSZ but the decrease is *very* small, from an average of 1.92 for the full catalogue, to an average of 1.86 for ϕ≥80%. Likewise, the increase in correlation of earthquakes separated by long interevent distances is such that $q_T(\Delta d$ >100km) is 1.63–1.79 when ϕ ≥70% and 1.63–1.89 when ϕ ≥80%. These results demonstrate that the dynamics fault networks and background seismogenetic processes in South California are sub-extensive and strongly correlated over all magnitude scales and interevent distances. Analogous effects have been observed in the crustal fault networks of North California (Efstathiou et al.; 2017) and continental Alaska (Tzanis et al., 2018).

Efstathiou et al., (2017) applied the methods employed herein to the analysis of the nature and dynamics of the North Californian seismogenetic systems, namely the Walker Lane – Sierra Nevada Range (henceforth SNR) and the north segment of the San Andreas Fault (henceforth nSAF). The results provided strong evidence of sub-extensivity albeit with different characteristics. The nSAF exhibited different behaviour with respect to the powerful (M7.2) Loma Prieta event of 1989. As can be seen in Fig. 14a and 14b, prior to that earthquake, nSAF was strongly correlated over all magnitude scales and interevent distances; *after* the earthquake it was found to be weakly correlated over all magnitude scales and all but the shortest and longest interevent distances. In this respect, nSAF exhibits evolutionary (self-o*rganizing*) Criticality without evident acceleration or deceleration of seismic release rates. The SNR system was found to be highly correlated over all analysable

magnitude scales (Fig. 14c) and interevent distances (Fig. 14d) and to exhibit attributes of quasi-stationary self-organized criticality.

When the results of the nSAF and sSAF full catalogues are compared in Fig. 14a and 14b, it is straightforward to see that the post-1990 dynamics of nSAF and the post-1980 dynamics of sSAF are very comparable, just as the post-1968 dynamics of sSAF also turn out to be. Notably, as of 1980 the sSAF system has not experienced any major earthquake northward of the US-Mexican border. The large Baja California event of 2010 (M7.1) ruptured the Laguna Salada fault (LSF), well to the south of sSAF. Although the LSF is a probable southward continuation of the Elsinore fault, it can easily be seen that any activity leading to, or following this event, does not appear to have influenced the dynamics of sSAF, which was demonstrably also not influenced by the Loma Prieta earthquake. Once again, one is tempted to ponder whether such "isolation" of the sSAF is effected by the Garlock and "Unspecified" seismic zones. When the analysis of the declustered nSAF catalogue (available only at the $\phi \geq 70\%$ probability level) is compared to the corresponding analysis of the declustered sSAF catalogue, it is easily verified that sSAF appears to be overall stronger correlated than nSAF, (Fig. 15a).

The results of the SNR and ECSZ full catalogues are compared in Fig. 14c and 14d. If only $q_T(M_{th})$ is considered, ECSZ appears to be significantly more correlated than the strongly correlated SNR. However, when $q_T(\Delta d)$ is only taken into consideration, SNR and ECSZ appear to be comparable with particular reference to the periods 1990-2011 for SNR and 1980-2017 for ECSZ. The largest part of this apparent discrepancy is due to the extensive and populous aftershock sequences of the 1992 Landers and 1999 Hector Mine events; the two systems turn out to be absolutely comparable when declustered realizations of the catalogues are considered, as in Fig. 15b which illustrates results for the $\phi \geq 70\%$ probability level. The two sibling systems can also be shown to be comparable at the $\phi \geq 80\%$ level: Efstathiou et al., (2017) determined a mean q_T of 1.76 in SNR for the period 1968-2011; herein we have determined an average of 1.86 (see above). Accordingly, the two subsystems of the Walker Lane zone are comparable although ECSZ appears to be somewhat stronger correlated than SNR.

It certainly stands to reason that the differences in the expression of seismicity between the sSAF/ICB and ECSZ networks, (and for that matter between nSAF/sSAF/ICB and SNR/ECSZ), reflect their respective niche in the geodynamic setting of the broader area. It is beyond the scope of this work to explore this fascinating problem. In any case, the evidence presented above indicates that they are certainly non-Poissonian. Foreground/background, as well as background seismicity is correlated and correlation increases with declustering in the southern segment of the San Andreas Fault system and the Inner Continental Borderland regions, or remains unabated in the Eastern California Shear Zone. This is a point of significance as it demonstrates that on muting the contribution of the correlated time-local foreground activity, the existence of long-range interaction in the background process becomes evident, as can be explicitly studied in Fig. 11 and 12. It should also be noted that even with full

(clustered) earthquake catalogues, correlation observed at interevent distances longer than 100km can hardly be explained in terms of aftershock sequences, as such ranges transcend the lengths of aftershock zones associated with M_w 7-7.3 earthquakes (e.g. Kagan, 2002). Another point of significance is that ETAS-based stochastic declustering *fails* to reduce earthquake catalogues to sequences of independent events. This should be emphasized because van Stiphout et al (2012) presented a study in which they compared declustering algorithms by applying the χ^2 goodness of fit test to determine whether the recovered "background" obeys a Poisson distribution with respect to time of occurrence; they found at the 5% significance level, that catalogues declustered by the method of Zhuang et al. (2002) do and on this basis they suggested that background dynamics are controlled by Poisson processes. We contend that this (and analogous) tests are misleading because the distribution of occurrence times is *not* a measure of dependence (interaction) between successive events whatsoever, and does not relate the occurrence of an earthquake to its predecessor and successor events. On the other hand, the distribution of interevent times does, as explained in the foregoing. Thus, when viewed in the context of NESP, our results indicate that background seismicity throughout South California expresses a set of persistently sub-extensive systems.

In concluding our presentation, we note that there are different mechanisms by which complexity and sub-extensivity may arise. To the extent that power-law distributions and long-range effects are hallmarks of critical phenomena, Self-Organized Criticality is by far the principal candidate. However, Complexity and Criticality do not always go hand in hand: there are non-critical mechanisms that may generate power-laws (e.g. Sornette, 2004; Sornette and Werner, 2009). In one such example, Celikoglu et al. (2010) demonstrated that the Coherent Noise Model (CNM) can generate *q*-exponential distributions of interevent times, although their simulation was incomplete in the sense that it did not include some spatial (geometric) configuration of interacting faults and could not assess the differences with an actual fault network. Our results may assist in understanding the origin of complexity in the fault systems of California. First, let us list some points that we consider significant:

a) It is evident that different, even adjacent fault networks may exhibit different attributes and degrees of complexity. This may indicate that in the case of Californian seismicity, models calling for uniform external driving forces that act upon all elements of a network, as for instance the CNM, may not be applicable at regional scales.
b) ECSZ and SNR exhibit persistent and strong long-range correlation during the 49 years since 1968. Far from suggesting that the state of strong correlation will endure "forever", we nevertheless point out that this quasi-stationary state has attributes of Self-Organized Criticality.
c) *Self-Organized* Criticality is not a general rule. This is evident in nSAF switching from a state of high correlation during the period leading up to the Loma Prieta event (1968-1989), to a state of low correlation in the period following that event (1990-2017). This shows that Criticality may be cyclic and possibly evolving in association with earthquake cycles. It also has attributes of the

Self-Organizing variety, albeit without evident acceleration of seismic release rates as predicted by some models (e.g. Sammis and Sornette, 2001).

d) There is (admittedly meagre) evidence that strong long-range correlation is also associated with increased localization of larger earthquake activity on larger faults: for instance, in sSAF, nSAF and SNR and for $M_{th} > 3.6$, the full-catalogue q_M increases steadily with threshold magnitude from approximately 1.5 (b=1) to approximately 1.59 ($b \approx 0.7$).

Based on such observations, we propose that a plausible interpretation for our results should involve fault networks with *small-world* topologies (e.g. Abe and Suzuki, 2004, 2007; Caruso et al., 2005, 2007). Given that active fault networks are *non-conservative* systems –friction is a non-conservative force– and therefore susceptible to non-linearity, we are pointed to this direction by the documented long-range interaction/ criticality, fruitful studies based on non-conservative small-world Olami-Feder-Christensen models (Caruso et al., 2005; Caruso et al., 2007), and suggestive evidence of small-worldness in the seismicity record of California by Abe and Suzuki (2004, 2007).

In such networks each fault is a node that belongs to a local cluster where it occupies some hierarchical level according to its size and interacts with local or distal faults (nodes) according to the connectivity and range of its hierarchical level. Upon excitation by some stress perturbation, a node responds by storing energy in the form of strain and subsequently transmitting it to *connected* nodes or/and releasing it at various rates; in other words, it operates as a delayed feedback loop inducing heterogeneity in the distribution of stress transfer and release rates. Finally and importantly, crustal fault networks are subject to free boundary conditions at the Earth-Atmosphere interface; top-tier faults, (which in transformational tectonic settings generally break at the surface), comprise primary boundary elements of the network.

It is documented that in Olami-Feder-Christensen networks, free boundary conditions compel the boundary elements to interact at a different (delayed) frequency with respect to the bulk of elements buried deeper in the network and that this induces partial synchronization of the boundary elements, building up long range spatial correlations and facilitating the development of a critical state (e.g. Lise and Paszucki (2002); Caruso et al., 2005; Hergarten and Krenn, 2011). In the particularly interesting study of Hergarten and Krenn (2011), the dynamics of the network are governed by two competing mechanisms: Synchronization, which is pushing the system to criticality, and de-synchronization which prevents it from becoming overcritical and generates foreshocks and aftershocks. Once the system has reached the critical state, synchronized failure transfers more stress to connected nodes and this causes them to fail early and globally, de-synchronizing with the rest of the system. If, however, time lag between de-synchronized failures is short, the system can re-synchronize and repeat the cycle. This mechanism generates sequences of foreshocks, main shocks and aftershocks. Notably, the notion that aftershocks are generated by de-synchronization due to large earthquakes is quite different –and more SOC– than that of the spontaneous triggering advocated by the ETAS model.

In consequence of the above, it is plausible that the small-world character and sub-extensive critical state of crustal fault networks along the transformational plate boundary of California is induced by the high connectivity of synchronised contiguous segments of the large transform faults. These may operate as "hubs" that facilitate longitudinal interactions (transfer of stress) between clusters but inhibit interactions between distal or unconnected networks that operate quasi-independently and develop different levels of self-organization, namely between nSAF and SNR as well as sSAF/ICB and ECZS. In addition, the intensity of the longitudinal interactions may vary in response to time-dependent changes in the external driving force and connectivity between hubs, as for instance may have happened to nSAF before and after the Loma Prieta event. The interpretation posits that free boundary conditions are central to the development of complexity and criticality. By inference, it also implies that deep-seated fault networks, as for instance in Wadati-Benioff zones, should be kept away from criticality as they are subject to fixed boundary conditions that inhibit synchronization. The results obtained for the Alaskan – Aleutian Arc deep (>40km) intermediate and deep seismicity appear to corroborate this proposition (Tzanis et al., (2018), as also does a preliminary analysis of deep seismicity in the NW Circum-Pacific Belt (Tripoliti, 2017). It remains to be seen with future research, whether our interpretation actually holds water.

Acknowledgments

This work was partly supported by the THALES Program of the Ministry of Education of Greece and the European Union in the framework of the project "Integrated understanding of Seismicity, using innovative methodologies of Fracture Mechanics along with Earthquake and Non-Extensive Statistical Physics – Application to the geodynamic system of the Hellenic Arc - SEISMO FEAR HELLARC".

References

Abe, S., and Suzuki, N., 2007. Dynamical evolution of clustering in complex network of earthquakes, Eur. Phys. J. B 59, 93–97; doi: 10.1140/epjb/e2007-00259-3

Abe, S., and N. Suzuki 2005. Scale-free statistics of time interval between successive earthquakes. Physica A, 350, 588-596.

Abe S., and Suzuki N., 2004. Complex Network of Earthquakes. In: Bubak M., van Albada G.D., Sloot P.M.A., Dongarra J. (eds) Computational Science - ICCS 2004. ICCS 2004. Lecture Notes in Computer Science, vol 3038. Springer, Berlin, Heidelberg; doi: 10.1007/978-3-540-24688-6_135

Abe, S., and Suzuki, N., 2003. Law for the distance between successive earthquakes, J. Geophys. Res., 108 (B2), 2113.

Astiz L. and Shearer M. P., 2000. Earthquake Locations in the Inner Continental Borderland, Offshore Southern California, Bulletin of the Seismological Society of America, 90 (2), 425–449.

Bak, P. and C. Tang, 1989. Earthquakes as a self-organized critical phenomenon. J. Geophys. Res., 94, 15635-15637.

Bak, P., Christensen, K., Danon, L. and Scanlon, T., 2002. Unified scaling law for earthquakes, Phys. Rev. Lett., 88, 178501; doi:10.1103/PhysRevLett.88.178501.

Bakar, B. and Tirnakli, U., 2009. Analysis of self-organized criticality in Ehrenfest's dog-flea model, Phys. Rev. E, 79, 040103; doi:10.1103/PhysRevE.79.040103.

Batak R. C and Kantz H., 2014. Observing spatio-temporal clustering and separation using interevent distributions of regional earthquakes, Nonlin. Processes Geophys., 21, 735–744; doi:10.5194/npg-21-735-2014.

Becker T.W., Hardebeck J.L. and Anderson G., 2005. Constraints on fault slip rates of the southern California plate boundary from GPS velocity and stress inversions, Geophys. J. Int., 160 (2), 634–650.

Caruso, F., Latora, V., Rapisarda, A. and Tadić, B., 2005. The Olami-Feder-Christensen model on a small-world topology, arXiv:cond-mat/0507643v1 [cond-mat.stat-mech] (last accessed December 2017).

Caruso, F., Pluchino, A., Latora, V., Vinciguerra, S. and Rapisarda, A., 2007: Analysis of self-organized criticality in the Olami-Feder-Christensen model and in real earthquakes, Phys. Rev. E, 75, 055101; doi: 10.1103/PhysRevE.75.055101.

Celikoglu, A., Tirnakli, U., and Duarte Queirós, S., 2010. Analysis of return distributions in the coherent noise model, Phys. Rev. E, 82, 021124; doi:10.1103/PhysRevE.82.021124.

Corral, A., 2004. Long-term clustering, scaling, and universality in the temporal occurrence of earthquakes, Phys. Rev. Lett., 92, 108501.

Davidsen, J. and Goltz, C., 2004. Are seismic waiting time distributions universal? Geophys. Res. Lett., 31, L21612; doi 10.1029/2004GL020892.

Dixon, T.H., Miller, M., Farina, F., Wang, H., and Johnson, D., 2000. Present-day motion of the Sierra Nevada block and some tectonic implications for the Basin and Range province, North American Cordillera, Tectonics, 19, 1–24; doi: 10.1029/1998TC001088.

Eaton J.P., 1992. Determination of amplitude and duration magnitudes and site residuals from short-period seismographs in Northern California, Bull. Seism. Soc. Am., 82 (2), 533-579.

Efstathiou A., Tzanis, A. and Vallianatos F., 2017. On the nature and dynamics of the seismogenetic systems of North California, USA: An analysis based on Non-Extensive Statistical Physics. *Physics of the Earth and Planetary Interiors*, 270, 46–72; doi: https://doi.org/10.1016/j.pepi.2017.06.010.

Efstathiou A., Tzanis, A. and Vallianatos F., 2016. On the nature and dynamics of the seismogenetic system of South California, USA: an analysis based on Non-Extensive Statistical Physics. *Bull. Geol. Soc. Greece*, 50 (3), 1329-1340; doi: http://doi.org/10.12681/bgsg.11839.

Efstathiou A., Tzanis A. and Vallianatos, F, 2015. Evidence of Non-Extensivity in the evolution of seismicity along the San Andreas Fault, California, USA: An approach based on Tsallis Statistical Physics, Phys. Chem. Earth, 85–86, 56–68; doi: http://doi.org/10.1016/j.pce.2015.02.013.

Eneva M. and Pavlis L. G, 1991. Spatial Distribution of Aftershocks and Background Seismicity in Central California, Pure and Applied Geophysics, 137 (1), 35-61.

Faulds, J.E., Henry, C.D., Hinz, N.H., 2005a. Kinematics of the northern Walker Lane: an incipient transform fault along the Pacific–North American plate boundary. Geology 33 (6), 505–508.

Faulds, J.E., Henry, C.D., Hinz, N.H., Drakos, P.S., Delwiche, B., 2005b. Transect across the Northern Walker Lane, northwest Nevada and northeast California: an incipient transform fault along the Pacific–North America plate boundary. In: Pederson, J., Dehler, C.M. (Eds.), Interior Western United States: Geol. Soc. Am. Field Guide, 6, 129–150; doi:10.1130/2005.fld006(06).

Felzer, K. R. and Brodsky, E. E. 2006 Evidence for dynamic aftershock triggering from earthquake densities, Nature, 441, 735-738.

Felzer, K. R., 2007. Stochastic ETAS Aftershock Simulator Program (AFTsimulator), available at http://pasadena.wr.usgs.gov/office/kfelzer/AftSimulator.html; last access December 2017.

Felzer, K. R., Becker, T. W., Abercrombie, R. E. , Ekstrom, G. and Rice J. R., 2002. Triggering of the 1999 Mw 7.1 Hector Mine earthquake by aftershocks of the 1992 Mw 7.3 Landers earthquake, J. Geophys. Res., 107, 2190; doi:10.1029/2001JB000911.

Fialko Y., 2006. Interseismic strain accumulation and the earthquake potential on the South San Andreas fault system, Nature, 441; doi:10.1038/nature04797, 968-971.

Gutenberg, R. and C.F. Richter (1944). Frequency of earthquakes in California, Bulletin of the Seismological Society of America, 34, 185-188.

Hainzl, S., Scherbaum, F. and Beauval, C., 2006. Estimating background activity based on interevent-time distribution, Bull. Seismol. Soc Am., 96 (1), 313–320; doi: 10.1785/0120050053.

Hardebeck, J. L., and. Hauksson E., 2001. Crustal stress field in southern California and its implications for fault mechanics, J. Geophys. Res., 106, 21,859–21,882.

Harry, D.L., 2005. Evolution of the western U.S. Walker Lane and East California shear zone: insights from geodynamic modeling. Geol. Soc. Am. Abstract with Programs 37 (7), 59.

Hauksson, E., Yang, W. and Shearer, P.M., 2012. Waveform Relocated Earthquake Catalog for Southern California (1981 to 2011), Bull. Seismol. Soc. Am., 102 (5), 2239-2244; doi:10.1785/0120120010

Hauksson E., 2010. Spatial Separation of Large Earthquakes, Aftershocks, and Background Seismicity: Analysis of Interseismic and Coseismic Seismicity Patterns in Southern California. In: Savage M.K., Rhoades D.A., Smith E.G.C., Gerstenberger M.C., Vere-Jones D. (eds), Seismogenesis and Earthquake Forecasting: The Frank Evison Volume II. Pure and Applied Geophysics, 167, 979-997; doi: 10.1007/s00024-010-0083-3.

Helmstetter, A. and Sornette, D., 2003. Predictability in the Epidemic-Type Aftershock Sequence model of interacting triggered seismicity, J. Geophys. Res., 108 (B10), 2482; doi:10.1029/2003JB002485.

Hergarten, S. and Krenn, R., 2011. Synchronization and desynchronization in the Olami-Feder-Christensen earthquake model and potential implications for real seismicity, Nonlin. Processes Geophys., 18, 635–642; doi:10.5194/npg-18-635-2011.

Jennings, C.W., 1994, Fault activity map of California and adjacent areas, with locations of recent volcanic eruptions: California Division of Mines and Geology Geologic Data Map 6, 92 p., 2 pls., scale 1:750,000.

Jones L.M, 1988. Focal Mechanisms and the state of San Andreas Fault in Southern California, J. Geophys. Res., 93 (B8), 8869-8891.

Kagan, Y.Y., 2002. Aftershock zone scaling, Bull. Seismol. Soc. Am., 92 (2), 641-655.

Li, Q., Liu, M., 2006. Geometrical impact of the San Andreas fault on stress and seismicity in California. Geophys. Res. Lett. 33, L08302; doi:10.1029/2005GL025661.

Lise, S. and Paczuski, M., 2002. A Nonconservative Earthquake Model of Self-Organized Criticality on a Random Graph, Phys. Rev. Lett., 88 (22), 228301; doi: 10.1103/PhysRevLett.88.228301

Liu M., Wang H. and Li Q., 2010. Inception of the Eastern California Shear Zone and evolution of the Pacific-North American plate boundary: From kinematics to Geodynamics; J. Geophys. Res., 115, B077401; doi: https://doi.org/10.1029/2009JB007055.

Martinez, M.D., Lana, X., Posadas, A.M. and Pujades, L., 2005. Statistical distribution of elapsed times and distances of seismic events: the case of the Southern Spain seismic catalogue,

Nonlinear Proc. Geophys., 12, 235–244.

Marzocchi, W. and Lombardi, A. M., 2008. A double branching model for earthquake occurrence, J. Geophys. Res., 113, B08317; doi:10.1029/2007JB005472.

McCrory, P.A., Wilson, D.S., Stanley, R.G., 2009. Continuing evolution of the Pacific–Juan de Fuca–North America slab window system — a trench–ridge-transform example from the Pacific Rim. Tectonophysics 464, 30–42. doi:10.1016/j.tecto.2008.01.018.

Miller, M.M., Johnson, D.J., Dixon, T.H., Dokka, R.K., 2001. Refined kinematics of the Eastern California shear zone from GPS observations, 1993–1998. J. Geophys. Res. 106 (B2), 2245–2263.

Molchan, G., 2005. Interevent time distribution in seismicity: A theoretical approach, Pure appl. geophys., 162, 1135–1150; doi: 10.1007/s00024-004-2664-5.

Moré, J.J. and Sorensen, D.C., 1983. Computing a Trust Region Step, SIAM Journal on Scientific and Statistical Computing, 3, 553–572.

Ogata, Y., 1998. Space-time point-process models for earthquake occurrences, Ann. I. Stat. Math., 50 (2), 379-402.

Ogata, Y., 1988. Statistical models for earthquake occurrences and residual analysis for point processes, J. Am. Stat. Assoc., 83 (401), 9-27.

Olami, Z., Feder, H. J. S., and Christensen, K.: Self-organized criticality in a continuous, nonconservative cellular automation modeling earthquakes, Phys. Rev. Lett., 68, 1244–1247, 1992

Plattner, C., Malservisi, R., Furlong K.P., Govers, R., 2010. Development of the Eastern California Shear Zone – Walker Lane belt: The effects of microplate motion and pre-existing weakness in the Basin and Range, Tectonophysics 485, 78–84; doi: https://doi.org/10.1016/j.tecto.2009.11.021.

Plattner, C., Malservisi, R., Govers, R., 2009. On the plate boundary forces that drive and resist Baja California motion. Geology 37, 359–362. doi:10.1130/G25360A.1.

Reasenberg, P. 1985. Second-order moment of central California seismicity, 1969-82, J. Geophys. Res., 90, 5479, 5495.

Rhoades, D. A., 2007. Application of the EEPAS model to forecasting earthquakes of moderate magnitude in Southern California, Seismol. Res. Lett., 78 (1), 110–115.

Rundle, J.B., Klein, W., Turcotte, D.L. and Malaud, B.D., 2000. Precursory seismic activation and critical point phenomena, Pure appl. Geophys., 157, 2165-2182.

Saichev, A. and Sornette, D., 2013. Fertility Heterogeneity as a Mechanism for Power Law Distributions of Recurrence Times, Physical Review E, 97, 022815; also available at arXiv:1211.6062 [physics.geo-ph] (last access December 2017).

Sammis, C.G. and Sornette, D., 2001. Positive feedback, memory and the predictability of earthquakes, e-print at http://arXiv.org/abs/cond-mat/0107143v1; last accessed December 2017.

Schoenball, M., N. C. Davatzes, and J. M. G. Glen, 2015. Differentiating induced and natural seismicity using space-time-magnitude statistics applied to the Coso Geothermal field, Geophys.Res. Lett., 42, 6221–6228; doi:10.1002/2015GL064772.

Segou, M., T. Parsons, and W. Ellsworth, 2013. Comparative evaluation of physics-based and statistical forecasts in Northern California, J. Geophys. Res. Solid Earth, 118, doi:10.1002/2013JB010313.

Silva, R., Franca, G.,S., Vilar, C.,S., Alcaniz, J.,S., 2006. Nonextensive models for earthquakes, Physical Review E, 73, 026102; doi:10.1103/PhysRevE.73.026102.

Sornette, A. and Sornette, D., 1989. Self-organized criticality and earthquakes, Europhys. Lett., 9,

197-202.

Sornette, D., 2004. Critical Phenomena in Natural Sciences: Chaos, Fractals, Self-organization and Disorder: Concepts and Tools, 2nd ed., 529 pp., Springer, Berlin

Sornette, D., and Sammis, C.G, 1995. Complex critical exponents from renormalization group theory of earthquakes: Implications for earthquake predictions, J. Phys. 1, 5, 607-619.

Sornette, D., and Werner, M.J., 2009. Statistical Physics Approaches to Seismicity, in Complexity in Earthquakes, Tsunamis, and Volcanoes, and Forecast, W.H.K. Lee (Ed), in the Encyclopedia of Complexity and Systems Science, R. Meyers (Editor-in-chief), 7872-7891, Springer, ISBN: 978-0-387-755888-6; available at arXiv:0803.3756v2 [physics.geo-ph] (last access December 2017).

Sotolongo-Costa, O. and Posadas, A., 2004. Tsalli's entropy: A non-extensive frequency-magnitude distribution of earthquakes. Phys. Rev. Letters, 92 (4), 048501; doi: 10.1103/PhysRevLett.92.048501.

Steihaug, T., 1983. The Conjugate Gradient Method and Trust Regions in Large Scale Optimization, SIAM J. Numer. Anal., 20, 626–637

Talbi, A. and Yamazaki, F., 2010. A mixed model for earthquake interevent times, J. Seismol, 14, 289–307; doi: 10.1007/s10950-009-9166-y.

Telesca, L., 2011. Tsallis-based nonextensive analysis of the Southern California seismicity. Entropy, 13, 1267-1280.

Telesca, L., 2012. Maximum Likelihood Estimation of the Nonextensive Parameters of the Earthquake Cumulative Magnitude Distribution, Bull. Seismol. Soc. Am., 102, 886-891

Touati, S., Naylor, M. and Main, I.G., 2009. Origin and Nonuniversality of the Earthquake Interevent Time Distribution, Phys. Rev. Letters, 102, 168501; doi: 10.1103/PhysRevLett.102.168501

Tripoliti, E., 2017. Evaluation of the nature of seismogenetic systems along the northwestern rim of the Circum-Pacific belt based on (non-extensive) statistical physics and complexity science methods, MSc Dissertation, National and Kapodistrian University of Athens, 119pp; https://pergamos.lib.uoa.gr/uoa/dl/object/1676052; accessed 3 August 2018.

Tsallis, C., 1988. Possible generalization of Boltzmann-Gibbs statistics, J. Stat. Phys., 52, 479–487; doi:10.1007/BF01016429

Tsallis, C., 2001. Nonextensive Statistical Mechanics and Thermodynamics: Historical Background and Present Status, in Abe, S. and Okamoto, Y (eds.), Nonextensive Statistical Mechanics and Its Applications, 3 – 98, Springer, Berlin , Heidelberg; doi: 10.1007/3-540-40919-X

Tsallis, C., 2009. Introduction to Nonextensive Statistical Mechanics: Approaching a Complex World. Springer Verlag, Berlin, 378pp.

Tsallis, C. and Tirnakli, U., 2010. Nonadditive entropy and nonextensive statistical mechanics – Some central concepts and recent applications, Journal of Physics: Conference Series 201 (2010) 012001; doi:10.1088/1742-6596/201/1/012001

Tzanis, A., Efstathiou, A. and Vallianatos, F., 2018. Are seismogenetic systems random or organized? A treatise of their statistical nature based on the seismicity of the north-northeast Pacific Rim. In Chelidze, T., Vallianatos, F. and Telesca, L. (eds), *Complexity of Seismic Time Series*, Elsevier, 365-418; doi: https://doi.org/10.1016/B978-0-12-813138-1.00011-0

Tzanis, A., Vallianatos, F. and Efstathiou, A., 2013. Multidimensional earthquake frequency distributions consistent with non-extensive statistical physics: The interdependence of Magnitude, Interevent Time and Interevent Distance in North California. *Bull. Geol. Soc. Greece*, 47 (3), 1326-1337. DOI: http://dx.doi.org/10.12681/bgsg.10914.

Uhrhammer B. R. A., Loper S. J., and Romanowicz B., 1996. Determination of local magnitude using BDSN Broadband Records, Bull. Seism. Soc. Am., 86 (5), 1314-1330.

Utsu, T.; Ogata, Y.; Matsu'ura, R.S., 1995. The centenary of the Omori formula for a decay law of aftershock activity, J. Phys. Earth, 43, 1–33.

van Stiphout, T., Zhuang J, and Marsan D., 2012, Seismicity declustering, Community Online Resource for Statistical Seismicity Analysis, doi: 10.5078/corssa-52382934. Available at http://www.corssa.org.

Weldon R., and E. Humphreys (1986). A kinematic model of southern California, Tectonics 5, 33–48.

Wernicke, B., Axen, G.J. and Snow J.K., 1988. Basin and Range extensional tectonics at the latitude of Las Vegas, Nevada, Geol. Soc. Am. Bull., 100 (11), 1738-1757; doi: 10.1130/0016-7606(1988)100<1738:BARETA>2.3.CO;2

Woessner, J., and S. Wiemer (2005). Assessing the quality of earthquake catalogues: Estimating the magnitude of completeness and its uncertainty, Bull. Seismol. Soc. Am., 95, 684–698; doi: 10.1785/0120040007

Zhuang J., Ogata Y. and Vere-Jones D., 2002. Stochastic declustering of space-time earthquake occurrences, J. Amer. Stat. Assoc., 97, 369-380.

TABLE 1

Table 1. Summary of the earthquake catalogues used in the present analysis.

Source Area	**Source Area Code**	**Period**	M_{comp}	**Full catalogues**	**Declustered catalogues** ($\phi_i \geq 70\%$)	**Declustered catalogues** ($\phi_i \geq 80\%$)	**Declustered catalogues** ($\phi_i \geq 90\%$)
				№ events	№ events	№ events	№ events
South California Seismic Region	**SCSR**	1968-2017	3.0	10,793	1,182	854	< 500
		1980-2017	2.5	30,117	4,224	3,081	2,035
San Andreas Fault South Segment	**sSAF**	1980-2017	2.5	17,602	2,468	1,767	1,619
East California Shear Zone South Segment	**ECSZ**	1980-2017	2.5	8,694	1,038	733	441
Inner Continental Borderline Offshore South California	**ICB**	1968-2017	2.5	3,821	694	< 500	< 300

TABLE 2

Table 2. Range of variation of the entropic indices obtained from the earthquake source areas of California.

		$q_T(M_{th})$ Range	$\langle q_T(M_{th})\rangle$	$q_T(\Delta d)$ Range		$q_M(M_{th})$ range	$\langle q_M(M_{th})\rangle$	$b_q(M_{th})$ range	$\langle b_q(M_{th})\rangle$	$q_M(\Delta d)$ Range	$b_q(\Delta d)$ range
				Δd<100km	Δd>100km						
FULL	**SCSR**	1.08-1.65	1.27±0.18	1.59	1.08-1.23	1.49-1.59	1.54±0.03	1.04-0.69	0.85±0.1	1.47-1.56	1.12-0.78
	sSAF	1.06-1.88	1.26±0.23	1.57-1.66	1.11-1.21	1.50-1.59	1.55±0.03	1.00-0.69	0.84±0.09	1.50-1.55	1.00-0.81
	ECSZ	1.79-1.98	1.92±0.07	1.59-1.95	1.67-1.70	1.48-1.53	1.51±0.01	1.08-0.88	0.96±0.03	1.48-1.52	1.08-0.92
	ICB	1.14-1.48	1.29±0.13	1.47-1.73	1.18-1.27	1.50-1.53	1.50±0.02	1.00-0.88	0.99±0.06	1.49-1.52	1.04-0.92
DECLUSTERED $\phi \geq 70\%$	**SCSR**	1.40-1.80	1.57±0.15	1.64	1.63-1.76	1.49-1.51	1.50±0.01	1.04-0.96	1.02±0.04	1.48-1.51	1.08-0.96
	sSAF	1.48-1.74	1.59±0.10	1.50	1.60-1.72	1.50-1.53	1.52±0.01	1.00-0.88	0.94±0.03	1.47-1.50	1.12-1.00
	ECSZ	1.62-1.79	1.74±0.06	-	-	1.49-1.52	1.51±0.01	1.04-0.92	0.95±0.05	-	
	ICB	1.71-1.80	1.75±0.06	-	-	1.50-1.52	1.51±0.01	1.00-0.94	0.98±0.04	-	
DECLUSTERED $\phi \geq 80\%$	**SCSR**	1.62-1.70	1.66±0.04	1.56	1.63-1.89	1.50-1.52	1.51±0.01	1.00-0.92	0.96±0.02	1.50-1.52	1.00-0.92
	sSAF	1.61-1.68	1.68±0.05	1.61	1.78-1.85	1.50-1.51	1.51±0.004	0.99-0.92	0.96±0.02	1.49-1.50	1.04-1.00
	ECSZ	1.83-1.88	1.86±0.03	-	-	1.50-1.52	1.51±0.01	1.00-0.92	0.97±0.04	-	
DECLUSTERED $\phi \geq 90\%$	**SCSR**	1.69-1.75	1.71±0.03	-	-	1.55-1.57	1.55±0.01	0.84-0.76	0.81±0.03	-	-
	sSAF	1.70-1.75	1.74±0.03	1.61	1.82	1.55-1.57	1.55±0.01	0.82-0.76	0.80±0.03	1.51-1.54	0.96-0.85

FIGURE 1

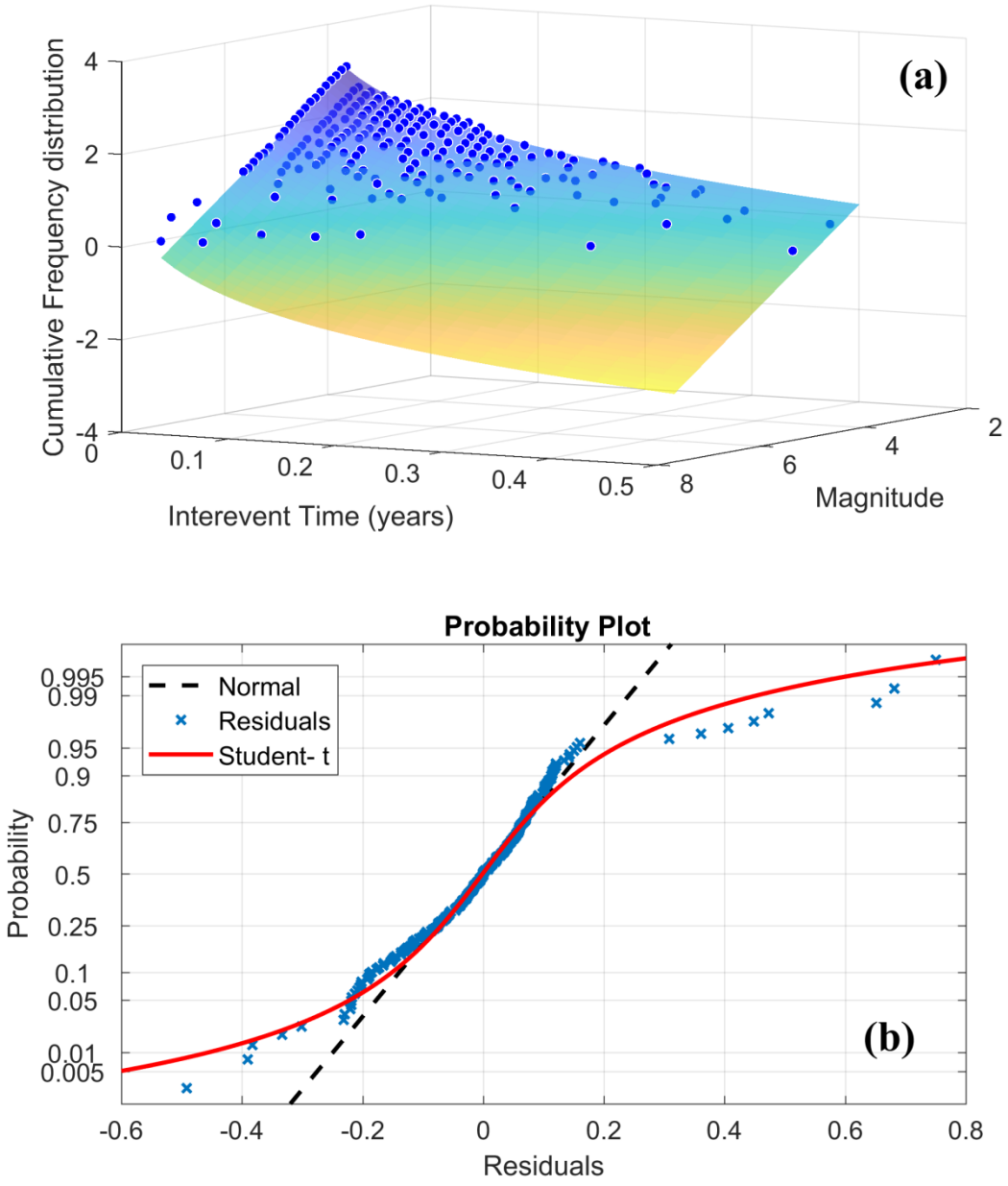

Figure 1: (a) The logarithm of an empirical F-M-T distribution (solid circles) and a model fitted using Eq. (7) and the Least Absolute Residual minimisation (transparent surface). **(b)** Probability analysis of the residuals computed by subtracting the model from the empirical F-M-T distribution (see text for details).

FIGURE 2

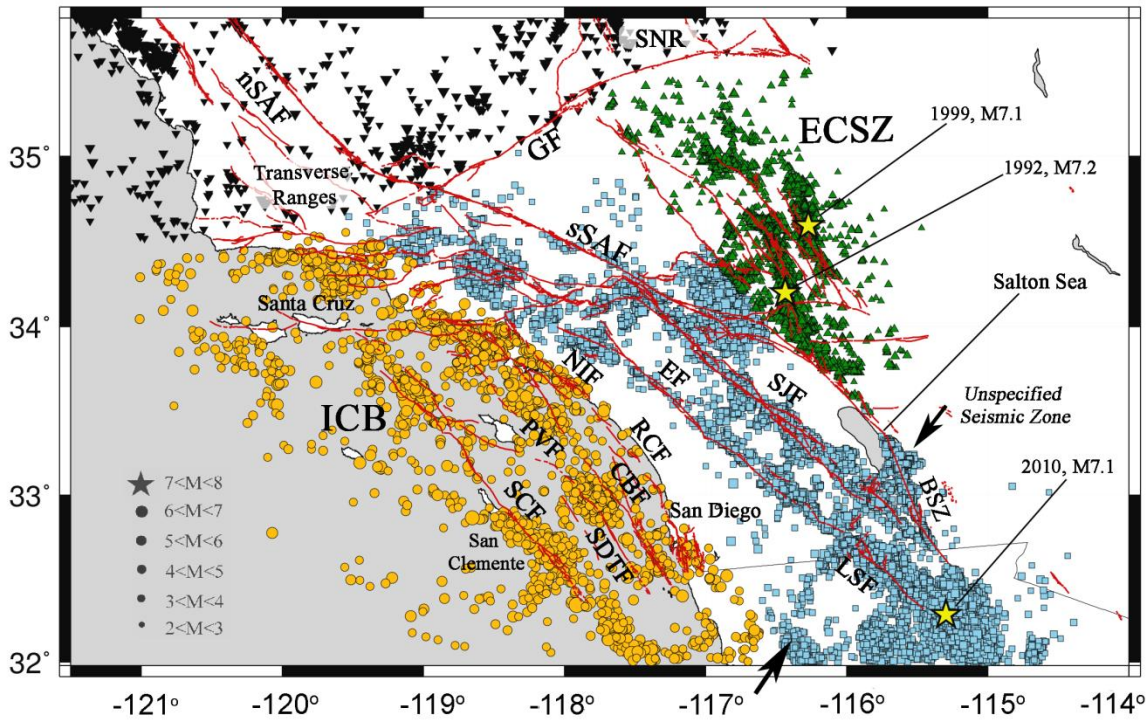

Figure 2. South California earthquake epicenters and major faults. **GF:** Garlock Fault; **ECSZ:** south segment of Eastern California Shear Zone; **nSAF:** north segment, San Andreas Fault; **SNR:** north segment of ECSZ; **sSAF:** south segment, San Andreas Fault; **SJF:** San Jacinto Fault; **EF:** Elsinore Fault; **BSZ:** Brawley Seismic Zone; **LSF:** Laguna Salada fault; **PVF:** Palos Verdes Fault; **NIF:** Newport-Inglewood fault; **RCF:** Rose Canyon fault. Offshore faults include the Coronado Bank Fault (**CBF**), San Diego Trough Fault (**SDTF**) and San Clemente Fault (**SCF**). The Transverse Ranges include the San Gabriel Fault, the San Cayetano Fault, the Oak Ridge Fault, and Santa Ynez Fault.

FIGURE 3

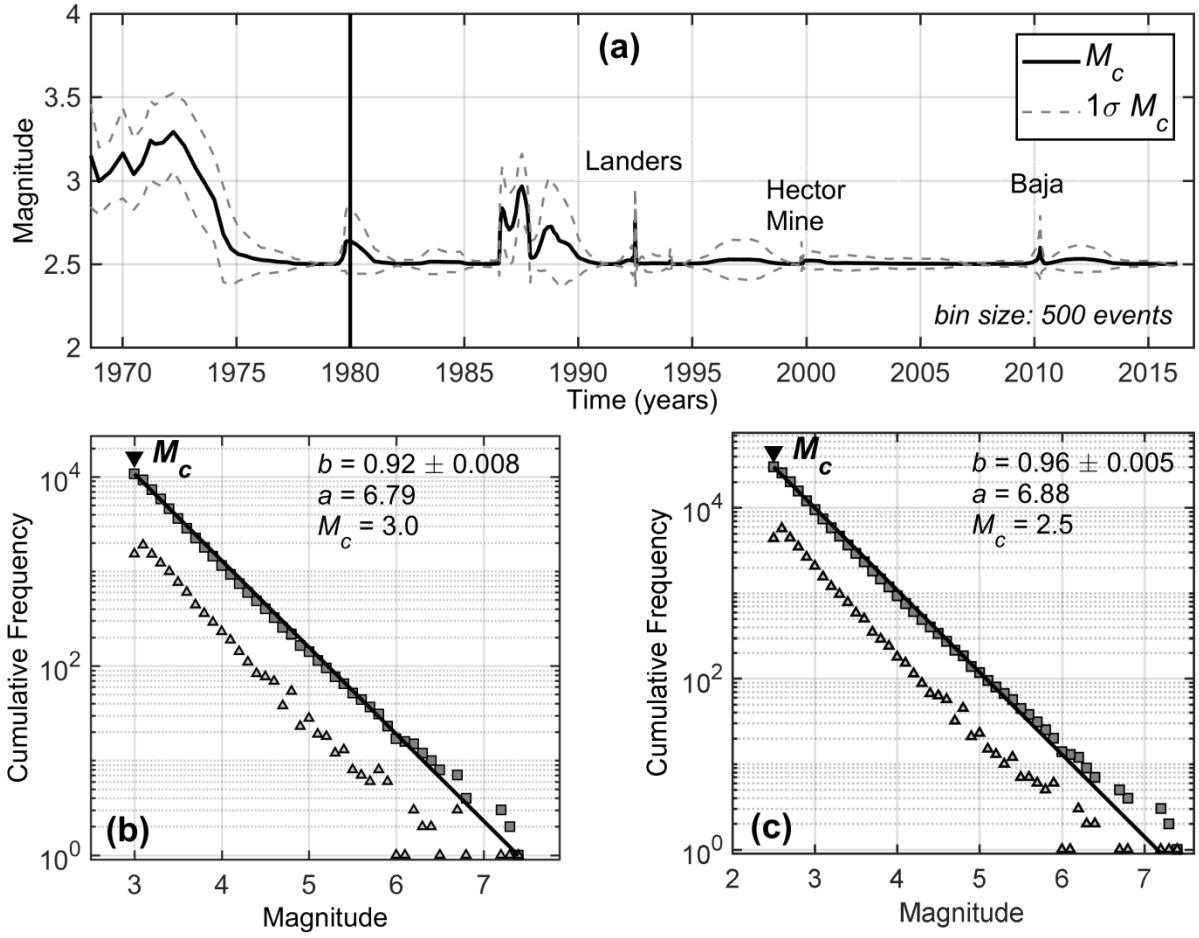

Figure 3 Attributes of SCSN earthquake catalogue: **a)** Magnitude of completeness (M_c) estimated as a function of time for the period 1968-2017 after Woessner and Wiemer (2005). **b)** Frequency – magnitude (F-M) distribution for the period 1968-2017; grey triangles denote the incremental distribution and grey squares the cumulative. **d)** As per Fig. 3b but for the period 1980-2017.

FIGURE 4

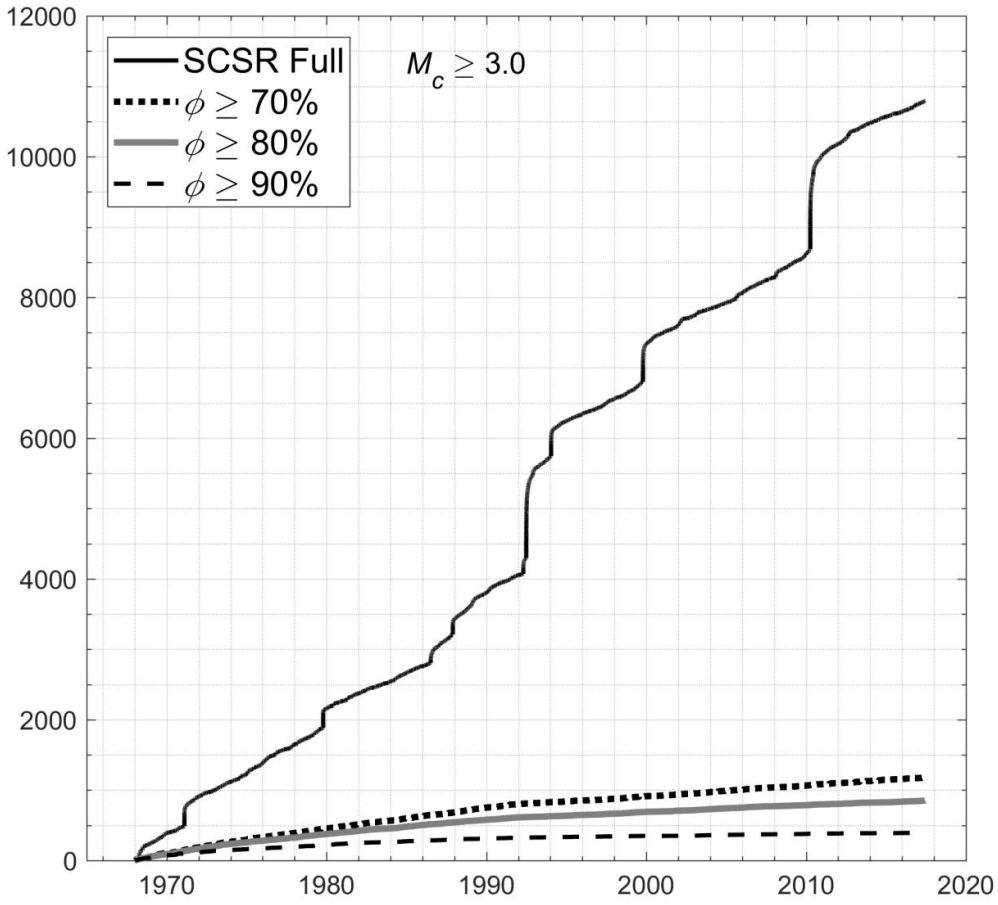

Figure 4: Cumulative event count of the full and declustered SCSN catalogue for the period 1968 – 2017 (magnitude of completeness $M_c \geq 3.0$).

FIGURE 5

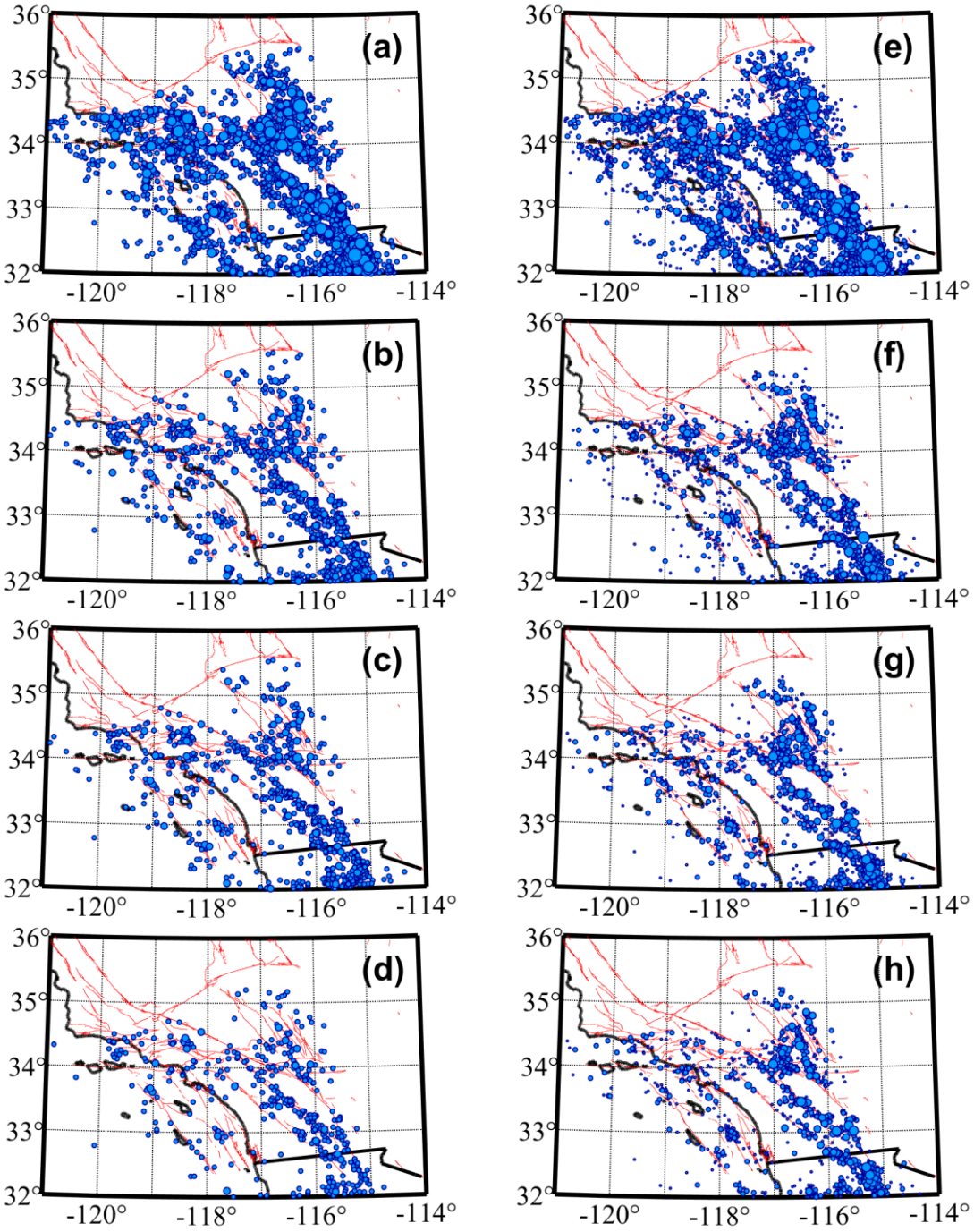

Figure 5: Epicentral maps of the full and declustered versions of the SCSN catalogue. **a)** Full catalogue for the period 1968-2017 and magnitude of completeness 3.0; **(b), (c)** and **(d)** declustered catalogue at probability levels 70%, 80% and 90% to be background respectively. **e)** Full catalogue for the period 1980-2017 and magnitude of completeness 2.5; **(f)**, **(g)** and **(h)** declustered catalogue at probability levels 70%, 80% and 90% to be background respectively.

FIGURE 6

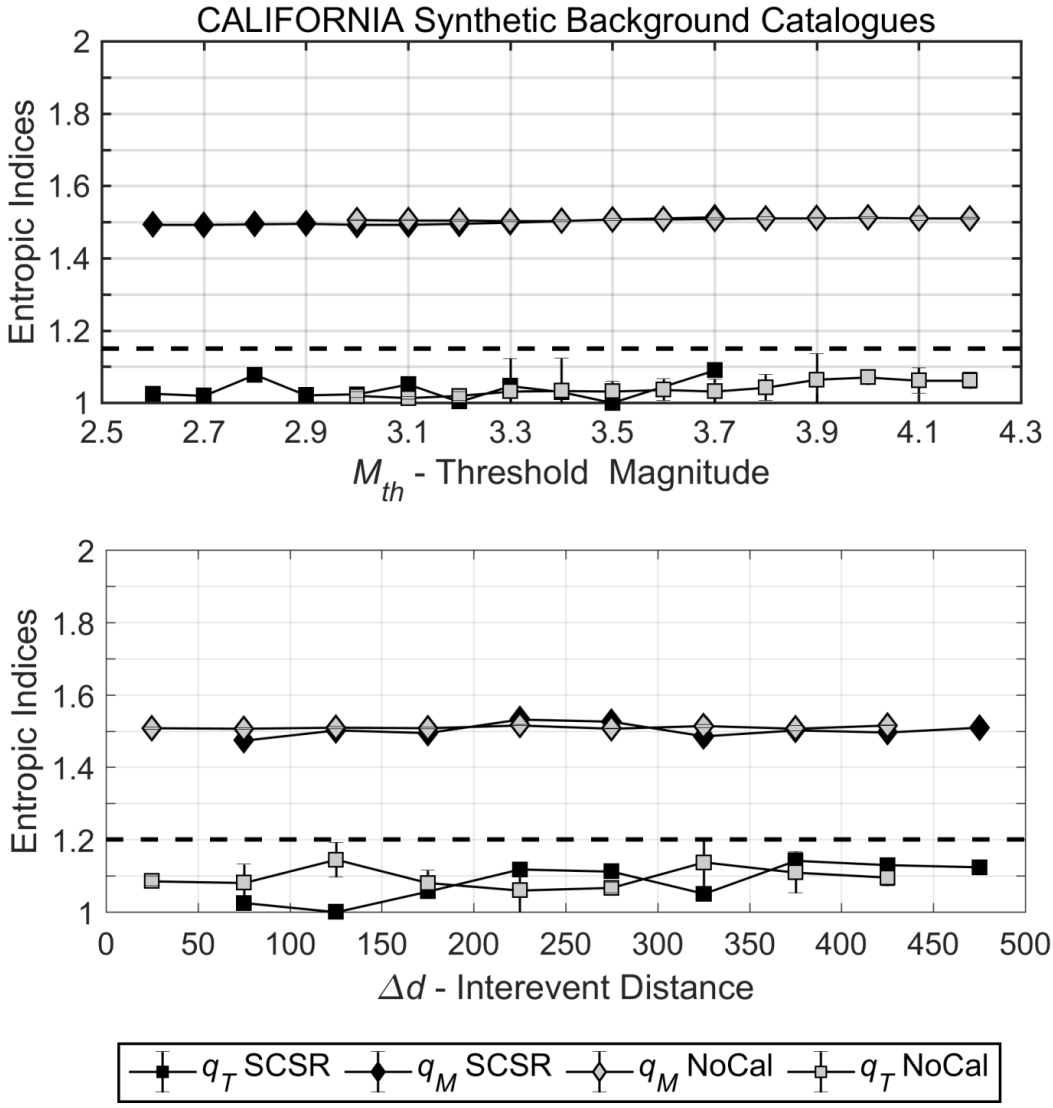

Figure 6: NESP analysis of 20 ETAS synthetic background catalogues constructed with the characteristics of South Californian (SCSR) and 20 constructed with those of North Californian seismicity (NoCal). Both span a period of 49 consecutive years. **(a)** Mean values $\langle q_T(M_{th})\rangle$ and $\langle q_M(M_{th})\rangle$ of the entropic indices and associated 3σ error, computed for different magnitude thresholds (M_{th}). The horizontal dashed line at q_T=1.15 marks the threshold above which $q_T(M_{th})$ can be *safely* assumed to represent non-Poissonian processes. **(b)** Mean values $\langle q_T(\Delta d)\rangle$ and $\langle q_M(\Delta d)\rangle$ with associated 3σ errors computed for different interevent distance groups Δd. The horizontal dashed line at q_T=1.2 marks the threshold above which $q_T(\Delta d)$ can be *safely* assumed to represent non-Poissonian processes.

FIGURE 7

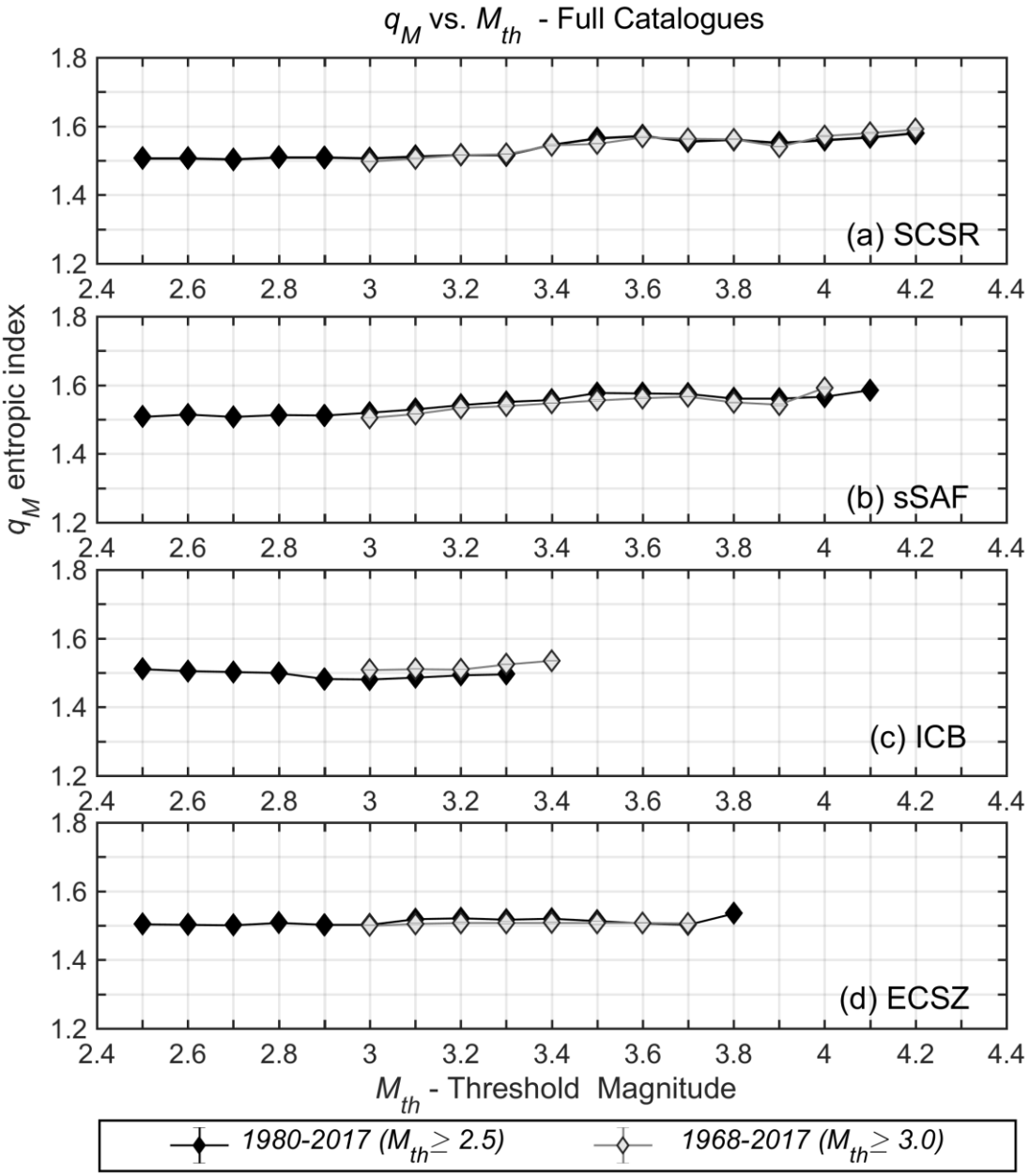

Figure 7. Variation of magnitude entropic indices (q_M) with threshold magnitude (M_{th}) for the full earthquake catalogues of: (a) the entire SCSR; (b) sSAF; (c) ICB, and, (d) ECSZ. 95% confidence limits are also drawn but are not always vissible as they usually are smaller than the symbols.

FIGURE 8

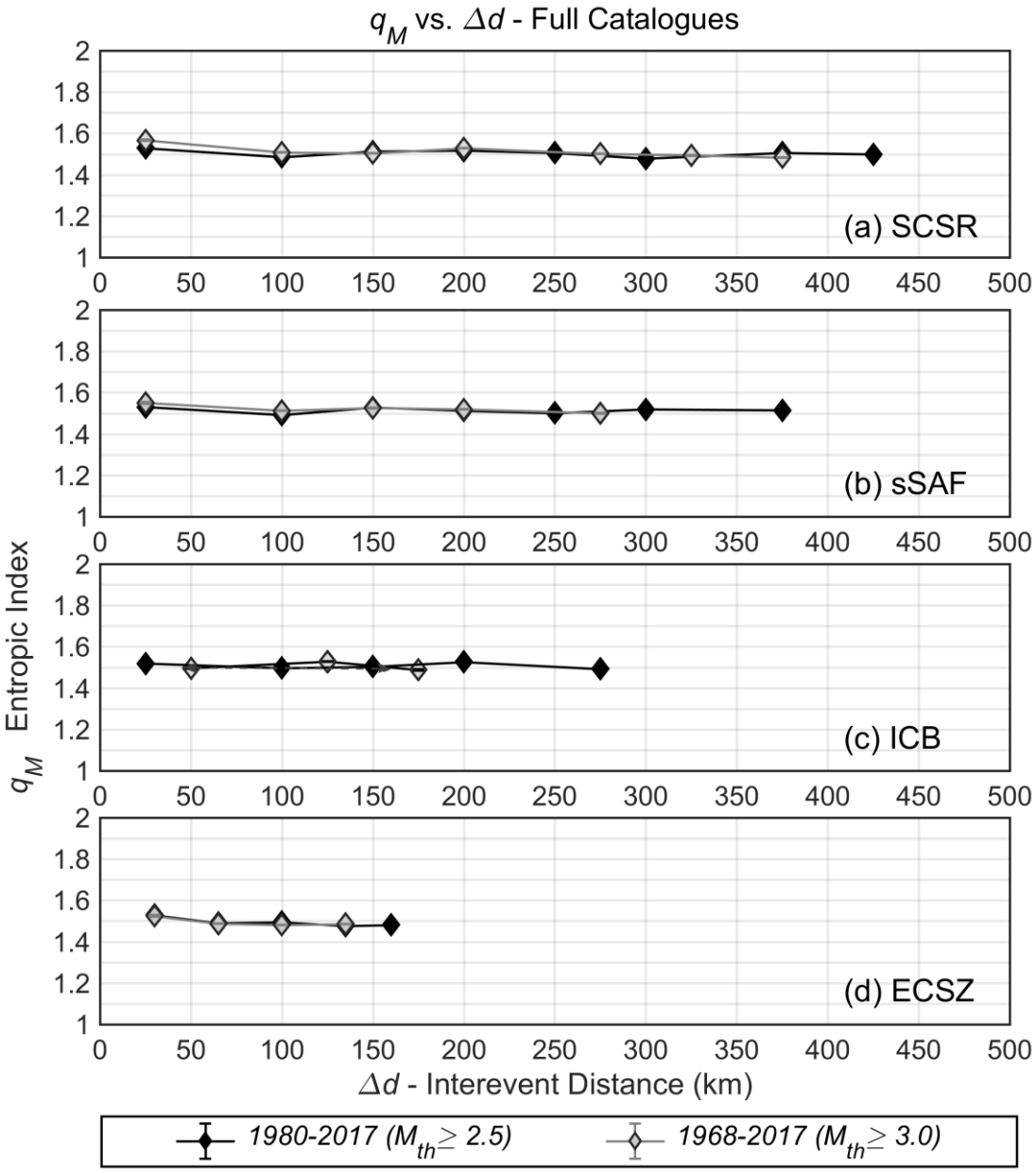

Figure 8. Variation of magnitude entropic indices (q_M) with interevent distance (Δd) for the full earthquake catalogues of: (a) the entire SCSR; (b) sSAF; (c) ICB, and, (d) ECSZ. Binning schemes (widths of interevent distance groups) vary and are selected so as to optimize goodness of fit. 95% confidence limits are also drawn but are not always vissible as they usually are smaller than the symbols.

FIGURE 9

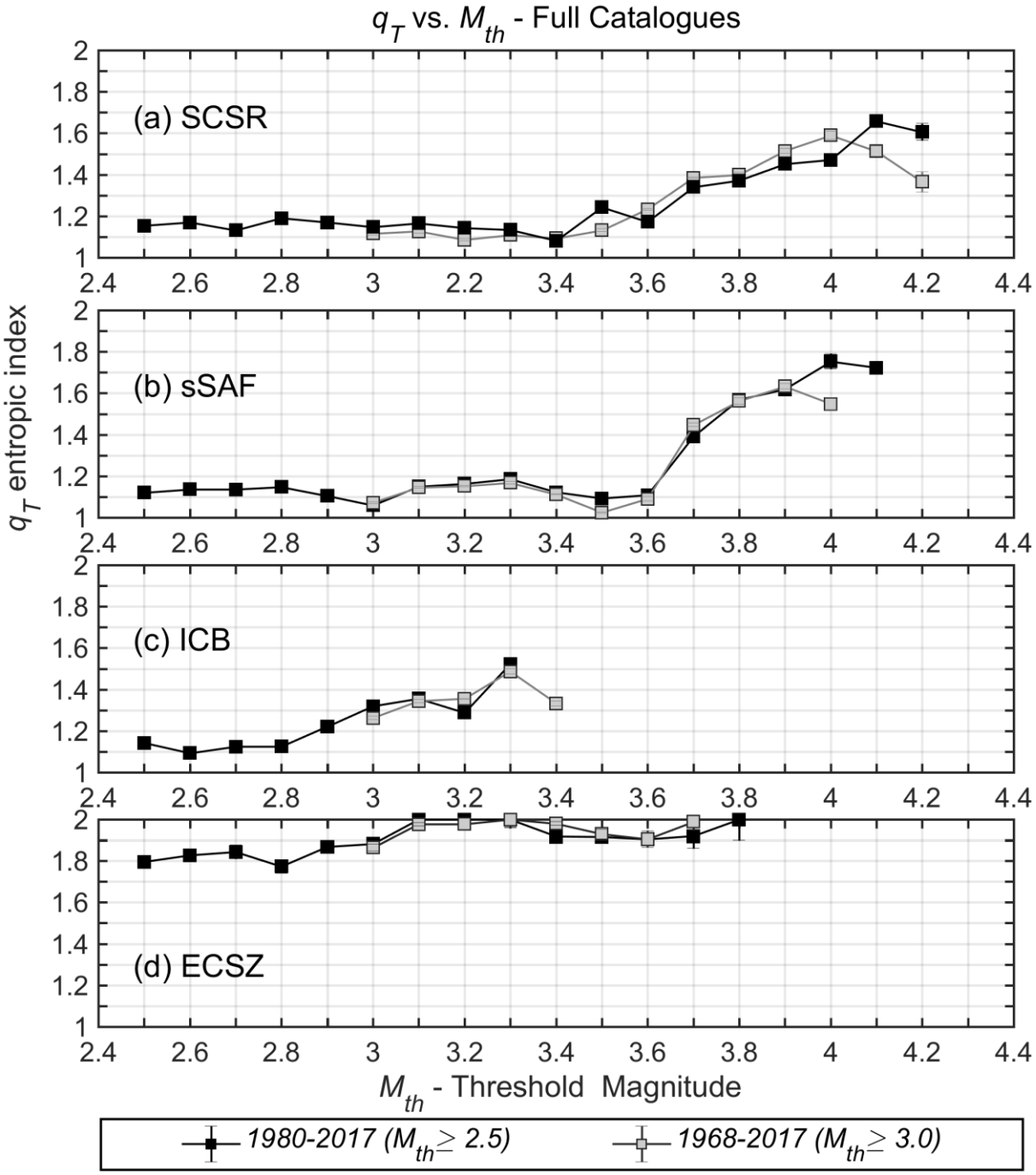

Figure 9. Variation of temporal entropic indices (q_T) with threshold magnitude (M_{th}) for the full earthquake catalogues of: (a) the entire SCSR; (b) sSAF; (c) ICB, and, (d) ECSZ. 95% confidence limits are also drawn but are not always vissible as they usually are smaller than the symbols.

FIGURE 10

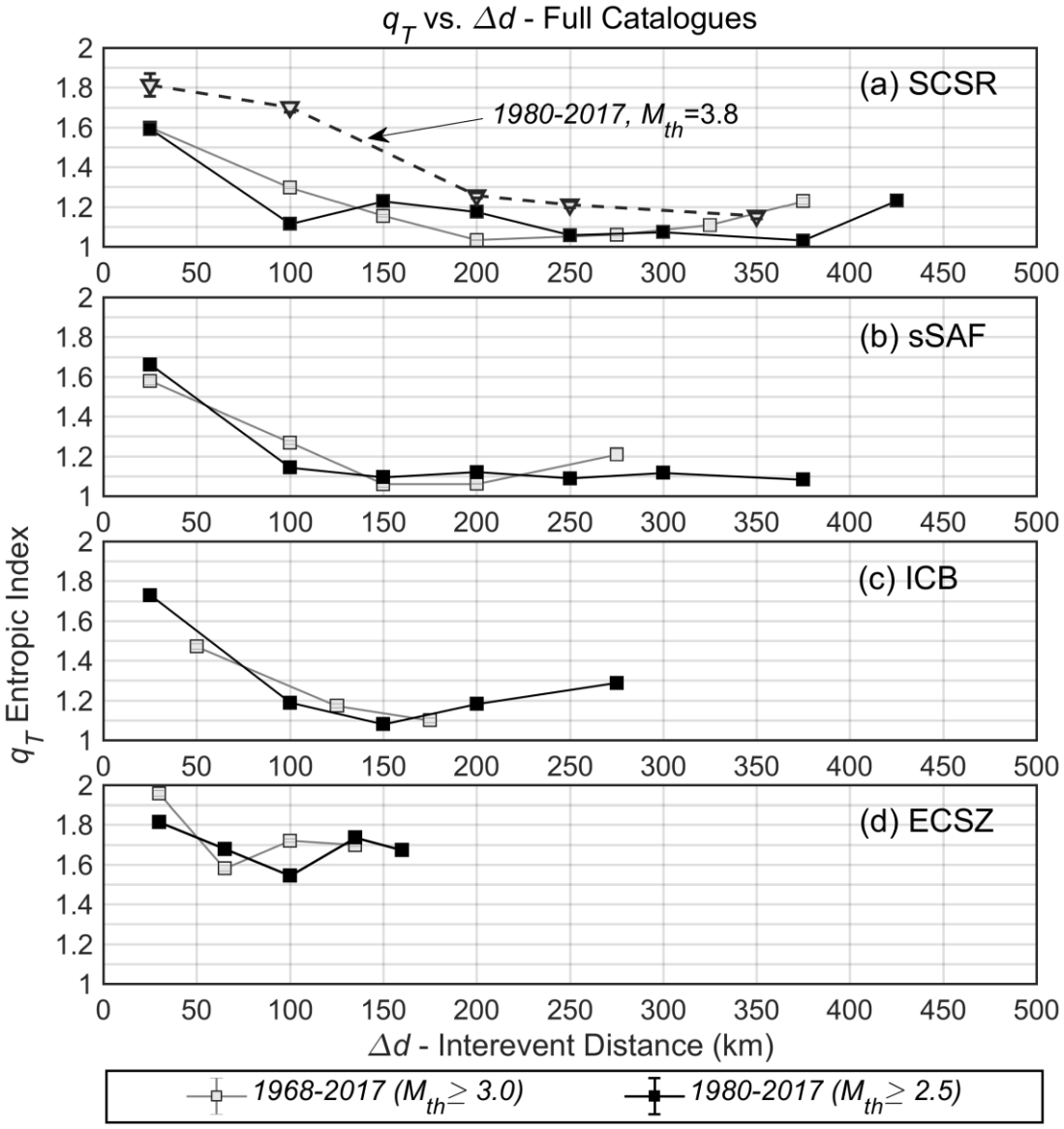

Figure 10. Variation of temporal entropic indices (q_T) with interevent distance (Δd) for the full earthquake catalogues of: (a) the entire SCSR; (b) sSAF; (c) ICB, and, (d) ECSZ. Binning schemes (widths of interevent distance groups) vary and are selected so as to optimize goodness of fit. 95% confidence limits are also drawn but are not always vissible as they usually are smaller than the symbols.

FIGURE 11

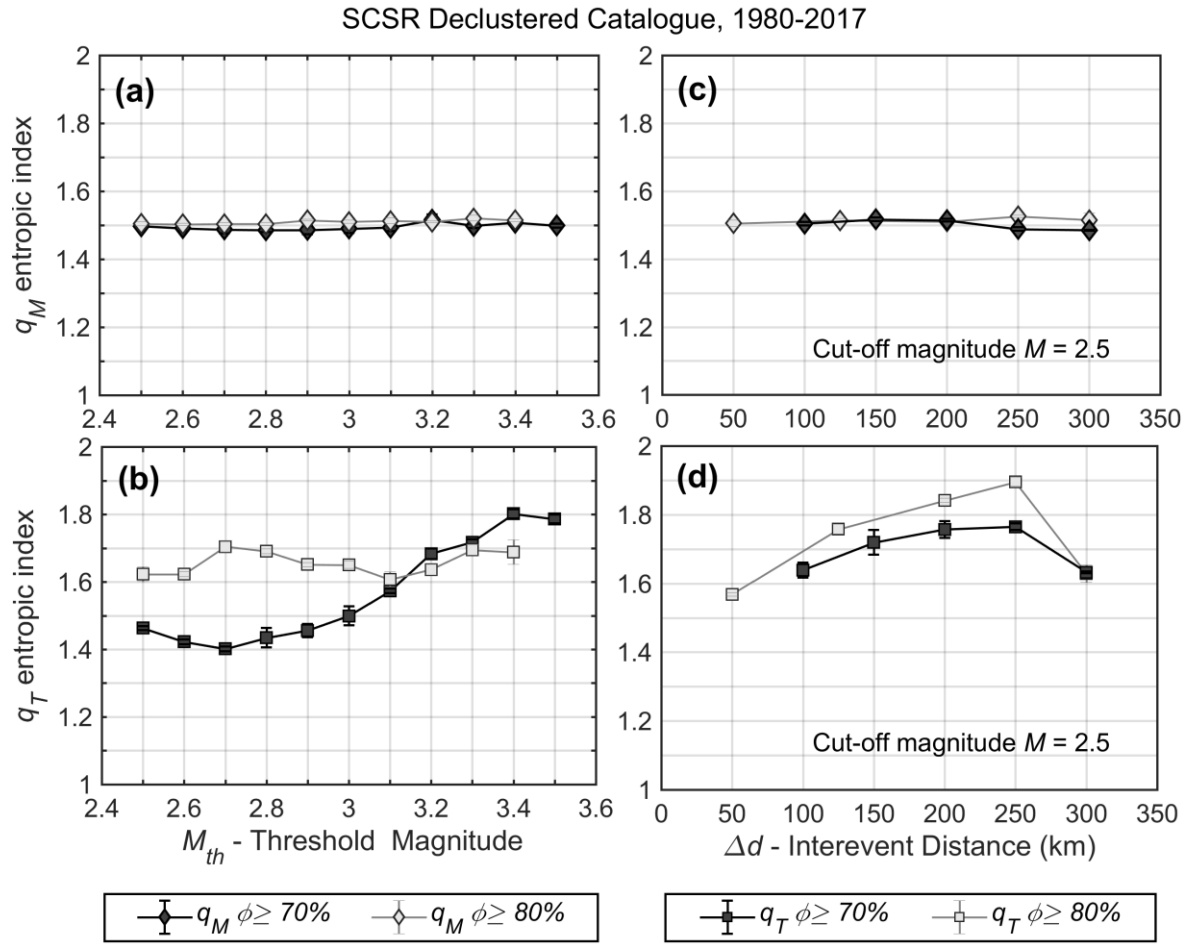

Figure 11. Analysis of the magnitude (q_M) and temporal (q_T) entropic indices for the catalogue of the South California Seismic Region *declustered* at probability levels 70% (dark colours) and 80% (light colours). **(a)** Variation of q_M with threshold magnitude (M_{th}); **(b)** Variation of q_T with threshold magnitude; **(c)** Variation of q_M with interevent distance (Δd); **(d)** Variation of q_T with interevent distance. In (c) and (d), binning schemes vary so as to maximize statistical rigour. Error bars represent 95% confidence limits; they are not always vissible as they frequently are smaller than the symbols.

FIGURE 12

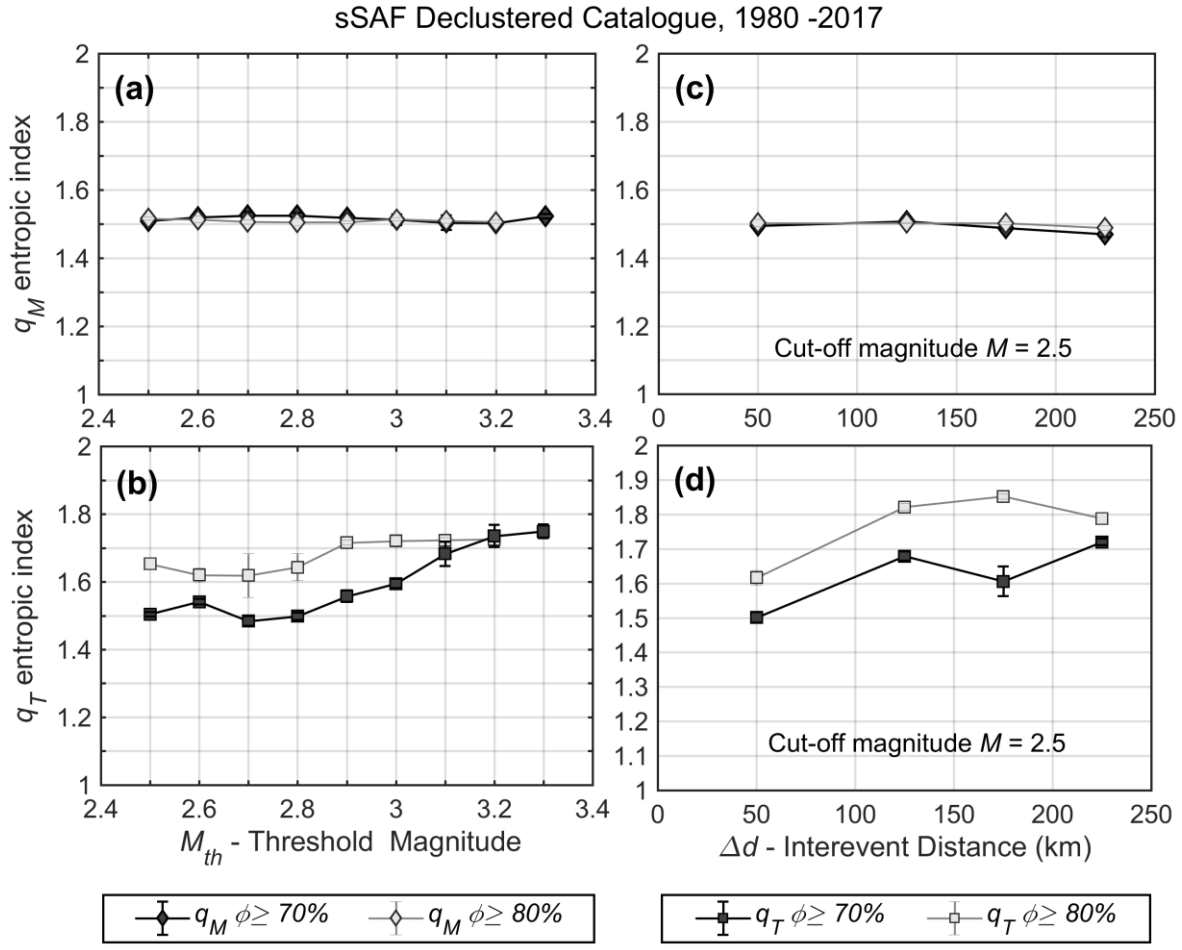

Figure 12. As per Fig. 11 but for the *declustered* catalogues of the south San Andreas Fault segment.

FIGURE 13

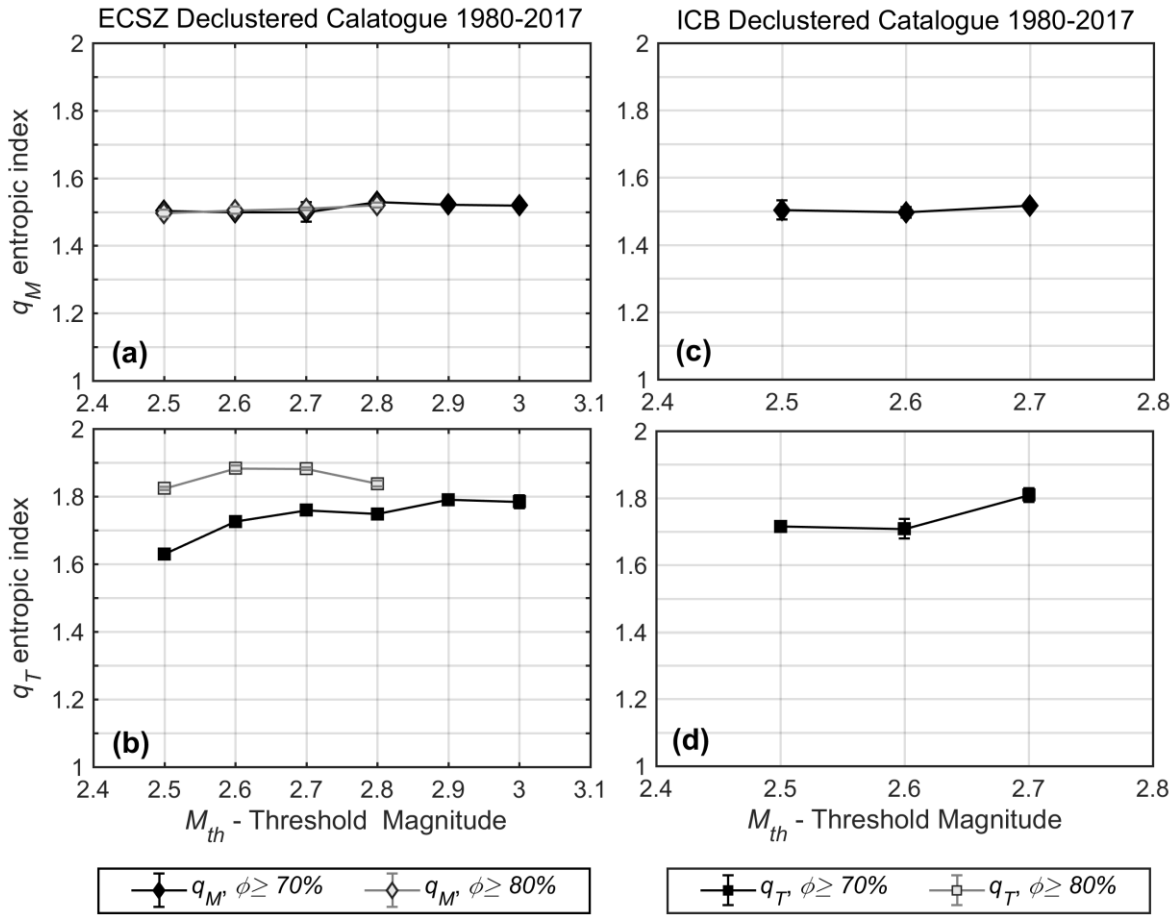

Figure 13. Variation of the magnitude (q_M) and temporal (q_T) entropic indices with threshold magnitude (M_{th}) for the declustered catalogues of the Eastern California Shear Zone (a, b) and the Inner Continental Borderland (c, d). Dark colours illustrate results obtained at the 70% background probability level; light colours results at the 80% probability level. Error bars represent 95% confidence limits; they are not always vissible as they frequently are smaller than the symbols.

FIGURE 14

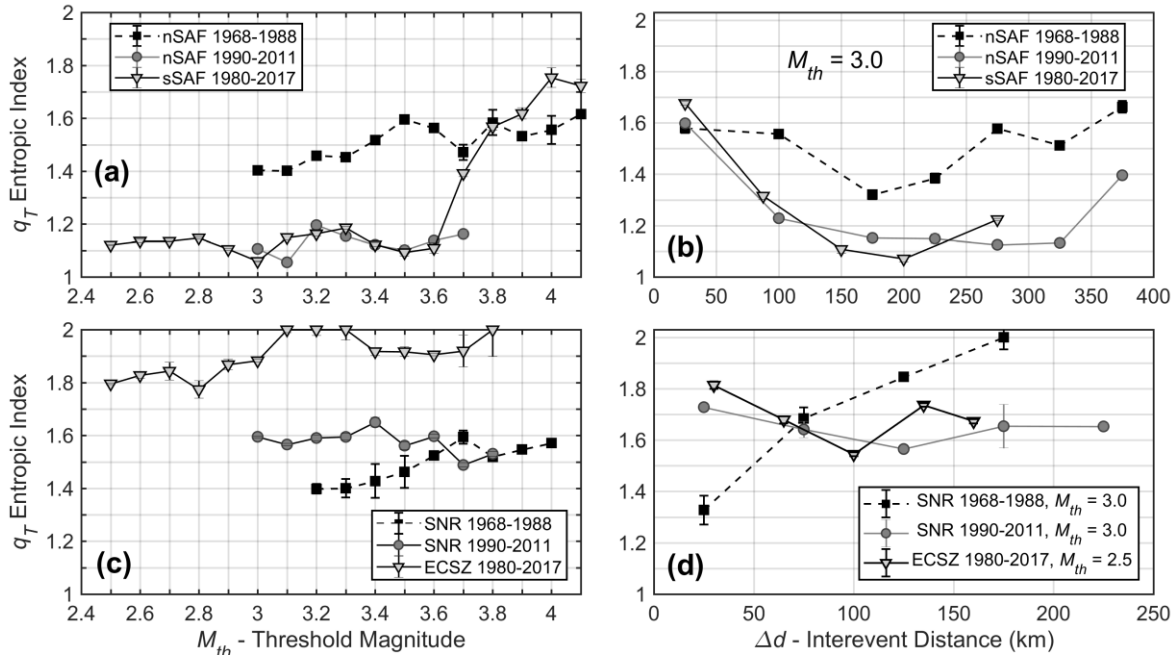

Figure 14: Comparison of $q_T(M_{th})$ and $q_T(\Delta d)$ obtained by Efstathiou et al. (2017) for the full catalogues of the seismogenetic systems in northern California with those obtained herein for southern California. **(a)** Comparison of $q_T(M_{th})$ for the northern (nSAF) and southern (sSAF) segments of the San Andreas Fault. **(b**) Comparison of $q_T(\Delta d)$ for nSAF and sSAF. **(c)** Comparison of $q_T(M_{th})$ for the Walker Lane – Sierra Nevada Range (SNR) and Eastern California Shear Zone (ECSZ). **(d)** Comparison of $q_T(\Delta d)$ for SNR and ECSZ.

FIGURE 15

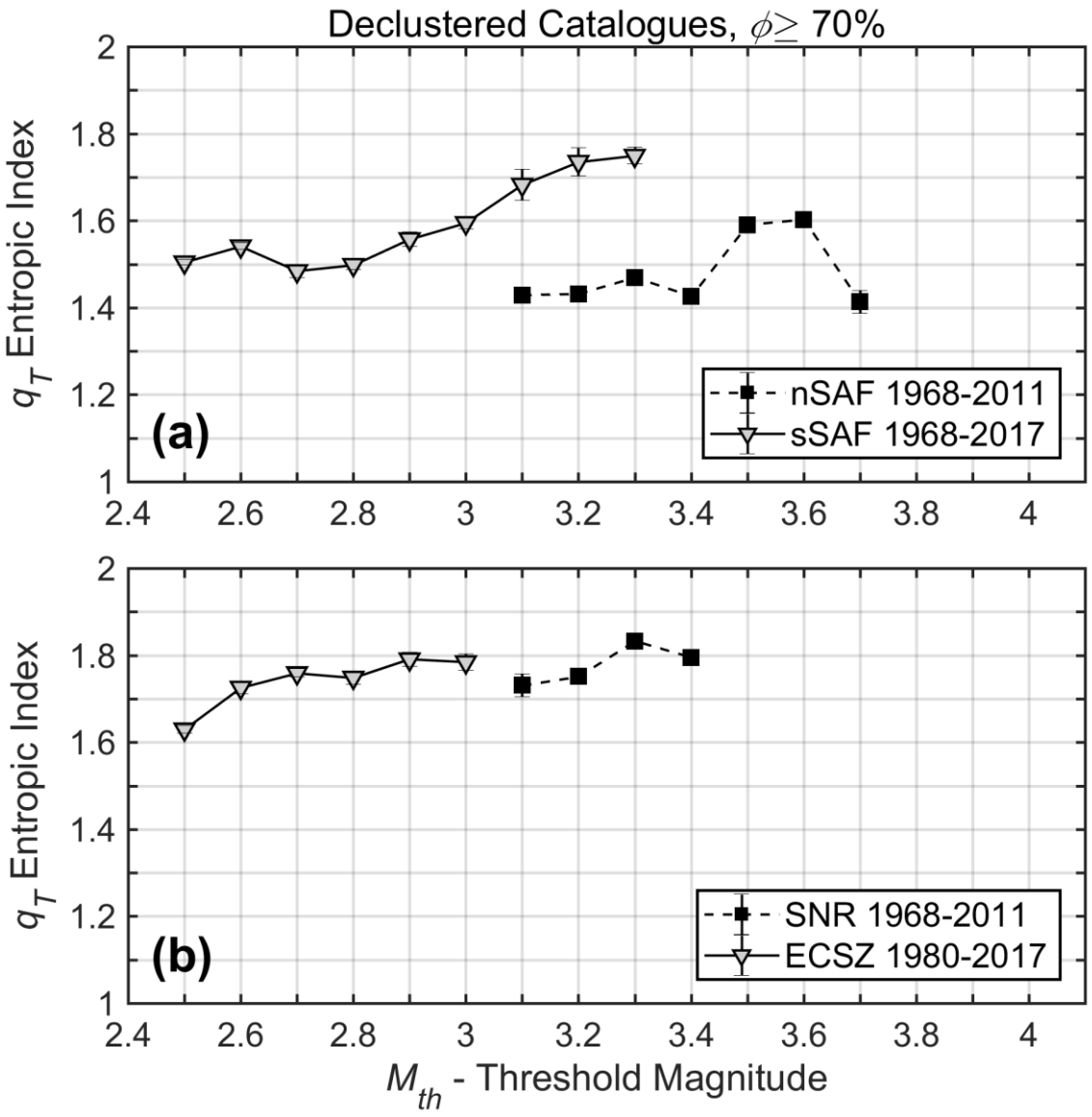

Figure 15: Comparison of $q_T(M_{th})$ obtained by Efstathiou et al. (2017) for *declustered* catalogues of the seismogenetic systems in northern California with those obtained herein for southern California ($\phi \geq 70\%$ probability level). **(a)** Comparison of the northern (nSAF) and southern (sSAF) segments of the San Andreas Fault. **(b**) Comparison of the Walker Lane – Sierra Nevada Range (SNR) and Eastern California Shear Zone (ECSZ).